AD-A260 391

MENTATION PAGE

Form Approved
OMB No. 0704-0188

1. AGENCY USE ONLY (Leave blank)	2. REPORT DATE	3. REPORT TYPE AND DATES COVERED
	January 6, 1993	FINAL REPORT 9-15-89 -- 9-14-92

4. TITLE AND SUBTITLE
Research in Photorefractive Crystals

5. FUNDING NUMBERS
DAAL03-89-K-0153

6. AUTHOR(S)
R. Hofmeister, A. Kewitsch, A. Agranat, A. Yariv

7. PERFORMING ORGANIZATION NAME(S) AND ADDRESS(ES)
California Institute of Technology
Pasadena, California 91125

8. PERFORMING ORGANIZATION REPORT NUMBER

9. SPONSORING/MONITORING AGENCY NAME(S) AND ADDRESS(ES)
U. S. Army Research Office
P. O. Box 12211
Research Triangle Park, NC 27709-2211

10. SPONSORING/MONITORING AGENCY REPORT NUMBER
ARO 27273.14-PH

11. SUPPLEMENTARY NOTES
The view, opinions and/or findings contained in this report are those of the author(s) and should not be construed as an official Department of the Army position, policy, or decision, unless so designated by other documentation.

12a. DISTRIBUTION/AVAILABILITY STATEMENT
Approved for public release; distribution unlimited.

12b. DISTRIBUTION CODE

13. ABSTRACT *(Maximum 200 words)*

Research in photorefractive materials in the last three years has involved the development of crystal growth techniques as well as characterization and applications of the grown materials. Potassium tantalate niobate (KTN) and potassium lithium tantalate niobate (KLTN) were grown.

14. SUBJECT TERMS
Photorefractive Crystals, photorefractive materials, crystal growth with KTN and KLTN

15. NUMBER OF PAGES
77

16. PRICE CODE

17. SECURITY CLASSIFICATION OF REPORT	18. SECURITY CLASSIFICATION	19. SECURITY CLASSIFICATION OF ABSTRACT	20 LIMITATION OF ABSTRACT
UNCLASSIFIED	UNCLASSIFIED	UNCLASSIFIED	UL

DISCLAIMER NOTICE

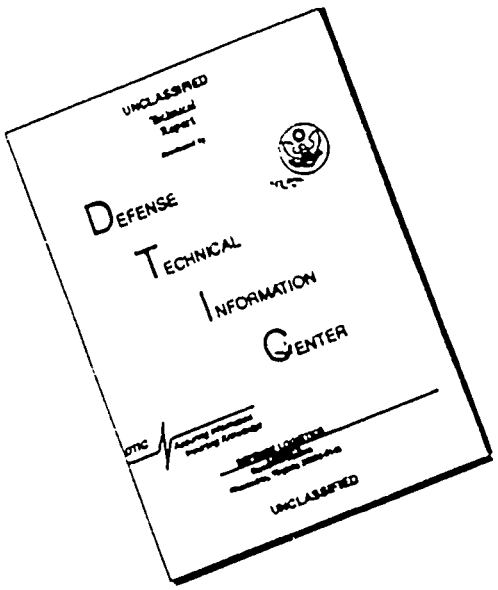

THIS DOCUMENT IS BEST QUALITY AVAILABLE. THE COPY FURNISHED TO DTIC CONTAINED A SIGNIFICANT NUMBER OF PAGES WHICH DO NOT REPRODUCE LEGIBLY.

RESEARCH IN PHOTOREFRACTIVE CRYSTALS

FINAL REPORT

R. Hofmeister, A. Kewitsch, S. Yagi, and A. Yariv

January 6, 1992

U.S. Army Research Office

DAAL03-89-K-0153

California Institute of Technology
Pasadena, California 91125

Approved for Public Release,
Distribution Unlimited

TABLE OF CONTENTS

Research in Photorefractive Crystals (DAAL03-89-K-0153)
Final Report November 1992

STATEMENT OF PROBLEM STUDIED:

Research in photorefractive materials in the last three years has involved the development of crystal growth techniques as well as characterization and applications of the grown materials. Potassium tantalate niobate (KTN) and potassium lithium tantalate niobate (KLTN) were grown.

SUMMARY OF MOST IMPORTANT RESULTS:

Crystal Growth:

A crystal growth system was constructed to use the *top seeded solution growth method.* Over 130 growths have been completed with this system; the crystals grown are generally of extremely high optical quality with dimensions of up to $20x15x15mm^3$. Efforts focused on enhancement of photorefractive properties by the selection of dopants introduced in the growth, and on the effects of lithium addition for KLTNs. We demonstrated that the dopants copper/vanadium and iron/titanium yielded exceptionally strong photorefractive response.

Recent efforts concentrated on the development of a KLTN with a phase transition temperature near room temperature, and on the complete elaboration of the growth process of KLTNs doped with copper vanadium. A series of crystals was grown with a constant lithium concentration and with progressively increasing niobium concentrations in an effort to raise the phase transition temperature. Then, when a fairly high atomic concentration of niobium was reached ([Nb] = .30), a series was grown with varying lithium concentration ([Li] = 0-0.12).

Material Characterization:

Several material properties of KTN/KLTN were examined. The results of dielectric measurements show that the transition temperature increases with increasing lithium or niobium concentration as expected. Thus we were able to obtain high quality KLTN crystals with phase transitions between 0-30°C with a

controllable lithium concentration. The growth parameters of KLTN:Cu, V were mapped out, and the phase diagrams established for various lithium concentrations. The results have been tabulated for over thirty separate compositions.

A study of the phase transition properties of the crystals with varying lithium concentrations was performed by measuring the low frequency dielectric constant versus temperature. We determined that for low concentrations of lithium, the transition is a ferroelectric one, and that multiple structural transitions occur at decreasing temperatures. This is as expected for a typical perovskite. As the lithium concentration is increased, however, the number of transitions decreases, first to two, then to one. Also, the nature of the transition seems to change to that of a so-called "spin glass." This effect has been observed by us at lower temperatures, but was for the first time seen at room temperature. These material studies were assisted by the use of electron microprobe and atomic absorption to determine crystal composition.

Photorefractive Properties:

The photorefractive properties of KTNs and KLTNs were studied in their high-temperature paraelectric phase. Here the crystals are centrosymmetric and do not display the conventional photorefractive effect unless an external field is applied. This allows the external modulation of the photorefractive effect. By applying a 0-2400V/cm electric field, we were able to obtain two-beam diffraction efficiencies of 0-75% in KLTN (60% in KTN). In addition, we demonstrated modulation of the photorefractive coupling at 20kHz.

Further studies showed that the photorefractive effect in the paraelectric phase was not exactly zero in the absence of an applied field. This was contrary to the conventional theory. We demonstrated that the effect, the Zero External Field Photorefractive (ZEFPR) effect, was due to a modulation of the strain field in the crystal by local Jahn-Teller relaxation of the $Cu^{2=}$ centers. This was proved to be a completely new effect with many important applications.

Using a crystal exhibiting the ZEFPR effect, we demonstrated the implementation of a novel all-optical microphone/vibration sensor. In addition, further applications are expected to include robust self=aligning holographic data links, self-aligning image subtraction

and processing devices, to name a few. These devices are the subject of a recently filed patent.

Theoretical Studies:

Several theoretical studies were conducted. We developed a method of solving certain types of linear coupled differential equations. We used this method to analyze photorefractive beam coupling in crystals. We have investigated the frequency reflectivity of fixed holograms for use as narrow-band interference filters. Also, the properties of dynamic holography during phase modulation of the interfering beams were studied. The particulars follow:

Two beam coupling in photorefractive crystals is described by well-known coupled mode equations. We have applied the theory to several new problems which are described here. First, we solve the coupled mode equations which gives the index modulation in the crystal. Then the resultant index grating is considered to be fixed, and reflection as a function of frequency is calculated. We were able to solve for the reflectivity for several experimental geometries (see Appendix A).

A similar theory was used to describe the effect of two beam coupling in a material with a fixed grating as described above. This theory was applied to describe the performance of the all-optical microphone/vibration sensor (see Appendix B).

Finally the theory was used to implement novel methods of determining the intrinsic phase in a photorefractive material. The phase in paraelectric KLTN was determined theoretically as a function of applied electric field. Both of these theories in conjunction were borne out experimentally (see Appendix C).

PUBLICATIONS AND TECHNICAL REPORTS:

R. Hofmeister, A. Yariv, and S. Yagi, "Spectrall Response of Fixed Photorefractive Grating Interference Filters" (See Appendix A).

R. Hofmeister and A. Yariv, "Vibration Detection Using Dynamic Photorefractive Gratings in KTN/KLTN Crystals" submitted for publications (see Appendix B).

R. Hofmeister, A. Yariv, A. Kewitsch and S. Yagi, "Simple Methods of Measuring the Photorefractive Phase Shift and Coupling Constant," submitted for publication (see Appendix C).

A. Agranat, R. Hofmeister and A. Yariv, "Characterization of a New Photorefractive Material: $K_{1-y}L_yT_{1-x}N_x$," Optics Letters, vol. 17, No. 10, pp. 713-715 (May 15, 1992) (see Appendix D).

R. Hofmeister, A. Yariv and S. Yagi, "New Photorefractive Mechanism in Centrosymmetric Crystals: A Strain-Coordinated Jahn-Teller Relaxation," Physical Review Letters, vol. 69, No. 9, pp. 1459-1462 (August 31, 1992) (see Appendix E).

SCIENTIFIC PERSONNEL WORKING ON THIS PROJECT AND DEGREES EARNED:

A. Yariv (Principal Investigator)
A. Agranat (Visiting Associate)
S. Yagi (Visiting Associate)
R. Hofmeister (Graduate Student)
A. Kewitsch (Graduate Student)

REPORT OF INVENTIONS:

DOCKET NO. 90-204 "Method and Apparatus for All-Optical Holographic Phase Modulation and Motion Sensing." (see Appendix F)

Spectral Response of Fixed Photorefractive Grating Interference Filters

Rudolf Hofmeister, Amnon Yariv, and Shogo Yagi*
California Institute of Technology
Pasadena, CA 91125

* permanent address NTT Interdisciplinary Research Laboratories
Ibaraki, Japan

Abstract

We report a theoretical investigation of the frequency response of optical interference filters written in photorefractive materials. Counterpropagating coherent beams interact in the volume of a photorefractive crystal through two-beam coupling. The resulting hologram is fixed. The reflectivity of the hologram is calculated as a function of frequency. An analytic solution is obtained for arbitrary grating phase ϕ in the lossless case, $\alpha = 0$. Numerical solutions are performed for $\alpha > 0$.

Introduction

Fixed photorefractive gratings have received interest recently for application as narrow-band optical interference filters and wavelength multiplexed optical memories[1,2,3,4]. The advantages of photorefractive filters over conventional methods are ease of fabrication and extremely narrow spectral response. We consider Bragg gratings which are written in a photorefractive material in exactly counterpropagating geometry. This method allows tuning the bandpass of the filter by adjusting the frequency of the laser writing beams. The index gratings written by the beams are then considered to be fixed by either thermal fixing or other methods. We calculate the spectral response of these filters to broadband or tunable incident radiation.

Theoretical Investigation, Lossless Case

We start by calculating the two beam coupling of two incident counterpropagating beams A(z) and B(z) in a photorefractive material. The well known coupled mode equations are[5]

$$A'(z) = \frac{i\pi\Delta n}{\lambda} e^{i\phi} B(z) \tag{1a}$$

$$B'(z) = \frac{-i\pi\Delta n^*}{\lambda} e^{-i\phi} A(z) \tag{1b}$$

where λ is the wavelength of the interfering beams, and the index of refraction is

$$n(z) = n_0 + \frac{1}{2}\left(\Delta n(z) e^{i\phi} e^{i\,2k\,z} + \text{c.c.}\right) \tag{2}$$

Here ϕ is the phase between the optical intensity grating and the induced index grating. This grating phase is an invariant property of the material. We require, without loss of generality, that B(z) be the amplified beam. That is, the propagation

direction of B(z) is nearer the z-axis than that of A(z). This is equivalent to restricting ϕ to the range $[0, \pi]$. Since the index grating is formed dynamically by the writing beams we have

$$\Delta n(z) = n_1 A(z)\ B^*(z)/I(z) \tag{3}$$

where I(z) is the total intensity, and n_1 is the peak-to-peak amplitude of the index grating when A(z) = B(z). Thus in the case of dynamic holography, the coupled mode equations can be simplified to

$$A'(z) = i\ g\ |B(z)|^2\ /I(z)\ e^{i\phi} A(z) \tag{4a}$$

$$B'(z) = -i\ g\ |A(z)|^2\ /I(z)\ e^{-i\phi} B(z) \tag{4b}$$

with $g = \pi n_1/\lambda$. We postulate solutions of the form

$$A(z)=a(z)e^{i\psi_1} \qquad B(z)=b(z)e^{i\psi_2} \tag{5}$$

where a(z)and b(z) are real. Equations 4a, b can be separated into two equations each describing the evolution of the amplitude and phase of the two beams.

$$a'(z) = -\sin\phi\, g\, |b(z)|^2 /I(z)\ a(z) \tag{6a}$$

$$b'(z) = -\sin\phi\, g\, |a(z)|^2 /I(z)\ b(z) \tag{6b}$$

$$\psi_1'(z) = \cos\phi\, g\, |b(z)|^2\ /I(z) \tag{7a}$$

$$\psi_2'(z) = -\cos\phi\, g\, |a(z)|^2\ /I(z) \tag{7b}$$

Equations 6a,b are solved by converting them to equations for intensities using $I_1' = (a^2)' = 2\,a\,a'$, and similarly for I_2. Simple Bernoulli equations are obtained with solutions

$$I_1(z) = \frac{1}{2}\left(\sqrt{c^2 + v^2 e^{-\Gamma z}} + c\right) \tag{8a}$$

$$I_2(z) = \frac{1}{2}\left(\sqrt{c^2 + v^2 e^{-\Gamma z}} - c\right) \tag{8b}$$

Here we have used the constants $\Gamma = 2g\sin\phi$, $c = I_1(z) - I_2(z)$ and $v^2 = 4\, I_1(0)\, I_2(0) = 4\, I_1(z)\, I_2(z)\, e^{\Gamma z}$. Also $I_1(z) = |A(z)|^2$ and $I_2(z) = |B(z)|^2$. In the case of equal intensity

inputs ($I_1(0) = I_2(L)$) these constants are given by $v^2 = 4I_1^2(0)\mathrm{Exp}[\Gamma L/2]/\mathrm{Cosh}[\Gamma L/2]$ and $c = -I_1(0)\mathrm{Tanh}[\Gamma L/2]$. The intensities are plotted in figure 1 for the case of equal intensity inputs, for g=20/cm, L=0.2cm, and several values of ϕ. The intensity coupling increases as the photorefractive phase ϕ deviates from zero. From the solutions in equations 8 we readily solve equations 7a,b to give

$$\psi_1(z) = \frac{1}{2}\left(g\cos\phi\, z - \cot\phi\, \coth^{-1}[\sqrt{1+(v/c)^2 e^{-\Gamma z}}]\right) \tag{9a}$$

$$\psi_2(z) = -\frac{1}{2}\left(g\cos\phi\, z + \cot\phi\, \coth^{-1}[\sqrt{1+(v/c)^2 e^{-\Gamma z}}]\right) \tag{9b}$$

Thus from equations 9, 8 and 5 we have solved the beam coupling in the counterpropagating geometry for arbitrary input beams and arbitrary material grating phase ϕ. The index grating in the material follows from equations 2 and 3 and is given by

$$\Delta n\, e^{i\phi} = n_1 \frac{v}{2} \frac{e^{-\Gamma z/2} + i\, g\cos\phi\, z + i\phi}{\sqrt{c^2+v^2 e^{-\Gamma z}}} \tag{10}$$

We note that the functional form of the index grating is simplified by the partial cancellation of the beam phases in equation 9. We plot the spatial variation of the magnitude of the index grating in figure 2 for the case of equal intensity inputs and for several values of ϕ.

We calculate the frequency reflectivity of an incident beam A(0) off this index grating. In analogy to equations 1a b we write the coupled mode equations

$$A'(z) = i\, g \frac{v}{2} \frac{e^{-\Gamma z/2} + i\, g\cos\phi\, z + i\phi}{\sqrt{c^2+v^2 e^{-\Gamma z}}}\, e^{-2i\,\Delta\beta\, z}\, B(z) \tag{11a}$$

$$B'(z) = -i\, g \frac{v}{2} \frac{e^{-\Gamma z/2} - i\, g\cos\phi\, z - i\phi}{\sqrt{c^2+v^2 e^{-\Gamma z}}}\, e^{+2i\,\Delta\beta\, z}\, A(z) \tag{11b}$$

where $\Delta\beta = (\omega_o - \omega)\, n_o / c$ is the frequency mismatch between the beams which wrote the grating and the one undergoing Bragg reflection. We have ignored the new dynamic grating which is written by the interference of the incident and

reflected beams since we are calculating the filter response to broadband illumination. Any such secondary grating would be bleached by the majority of light which is not reflected. In equations 11, B(z) is the reflected beam so that we take B(L) = 0, where L is the length of the crystal.The analytic solution of equations 11 subject to this boundary condition follows.

We first note that equations 11a and b can be written in the form

$$A'(z) = g(z)\, f(z)\, B(z) \tag{11c}$$

$$B'(z) = [g(z)/f(z)]\, A(z) \tag{11d}$$

where $f(z) = i \exp[-2i\Delta\beta z]$. We can eliminate g(z) by performing the independent variable transformation of z to ξ where

$$\xi = -\frac{\Gamma v}{2c}\int \frac{e^{-\Gamma z/2}}{\sqrt{1+(v/c)^2 e^{-\Gamma z}}}\, dz = \sinh^{-1}[\frac{v}{c}e^{-\Gamma z/2}] \tag{12}$$

The result is a set of coupled equations in ξ:

$$a'(\xi) = \frac{\kappa}{2}\, f(\xi)\, b(\xi) \tag{13a}$$

$$b'(\xi) = \frac{\kappa^*}{2}\, f^*(\xi)\, a(\xi) \tag{13b}$$

where

$$f(\xi) = \left(\frac{c}{v}\sinh[\xi]\right)^{4\, i\, \Delta\beta'/\Gamma} \tag{14}$$

$$\kappa = -i\, e^{i\phi}/\sin\phi \tag{15}$$

and $\Delta\beta' = \Delta\beta - (g/2)\cos\phi$.

In order to convert the above into solvable second order equations we derive the following general "corotating" transformation. Consider coupled differential equations of the form

$$a'(z) = \kappa\, f(z)\, b(z) \tag{16a}$$

$$b'(z) = \kappa^*/f(z)\, a(z) \tag{16b}$$

Note that we derive the following transformation for arbitrary f(z), not just as in equations 13 for which $1/f(z) = f^*(z)$. If we define

$$a(z) = T(z)\, e^{iF(z)} \quad \text{and} \quad b(z) = V(z)\, e^{-iF(z)} \tag{17}$$

where $$F(z) = 1/(2i)\, \mathrm{Log}[f(z)], \tag{18}$$

we can obtain

$$T''(z) = \left[|\kappa|^2 - \left(F'(z)\right)^2 - iF''(z)\right] T(z) \tag{19a}$$

$$V''(z) = \left[|\kappa|^2 - \left(F'(z)\right)^2 + iF''(z)\right] V(z) \tag{19b}$$

Here F(z) has been chosen so as to eliminate the first derivative terms in the second order equations. If this transformation is applied to equations 13 it yields

$$T''(\xi) + \left(\frac{-1}{4\sin^2\phi} + \eta^2 - \frac{i\eta(i\eta+1)}{\sinh^2\xi}\right) T(\xi) = 0 \tag{20a}$$

$$V''(\xi) + \left(\frac{-1}{4\sin^2\phi} + \eta^2 - \frac{i\eta(i\eta-1)}{\sinh^2\xi}\right) V(\xi) = 0 \tag{20b}$$

where we define $\eta = 2\Delta\beta'/\Gamma$. These are examples of the second Pöschl-Teller equation which has previously been solved[6,7].

Using reference 6 we obtain a solution for T(ξ) and V(ξ), and using equations 17, 12, and 13 we get

$$A(z) = \sqrt{1+\left(\frac{v}{c}\right)^2 e^{-\Gamma z}} \left\{ C_1\, {}_2F_1\left[\frac{1}{2} - i\frac{\eta}{2} - i\beta, \frac{1}{2} - i\frac{\eta}{2} + i\beta; \frac{1}{2} - i\eta; -\left(\frac{v}{c}\right)^2 e^{-\Gamma z}\right] + \right.$$
$$\left. C_2 e^{-(1+2i\eta)\Gamma z/2}\, {}_2F_1\left[-i\frac{\eta}{2} - i\beta + 1, -i\frac{\eta}{2} + i\beta + 1; \frac{3}{2} + i\eta; -\left(\frac{v}{c}\right)^2 e^{-\Gamma z}\right] \right\} \tag{21a}$$

$$B(z) = \sqrt{1+\left(\frac{v}{c}\right)^2 e^{-\Gamma z}} \left\{ C_3 e^{-(1-2i\eta)\Gamma z/2}\, {}_2F_1\left[-i\frac{\eta}{2} - i\beta + 1, -i\frac{\eta}{2} + i\beta + 1; \right.\right.$$
$$\left.\left. \frac{3}{2} - i\eta; -\left(\frac{v}{c}\right)^2 e^{-\Gamma z}\right] + C_4\, {}_2F_1\left[i\frac{\eta}{2} - i\beta + \frac{1}{2}, i\frac{\eta}{2} + i\beta + \frac{1}{2}; \frac{1}{2} + i\eta; -\left(\frac{v}{c}\right)^2 e^{-\Gamma z}\right] \right\} \tag{21b}$$

where

$$\beta = \frac{1}{2}\sqrt{\left|\frac{1}{4\sin^2\phi} - \eta^2\right|} \tag{22}$$

and C_1, C_2, C_3, C_4 are constants. We determine the constants from the boundary condition B(L)=0 and equations 11. The result is

$$C_1 = \frac{A(0)4\sin^2\phi\,(1+4\eta^2)}{\sqrt{1+(v/c)^2}} e^{(1-2i\eta)\Gamma L/2} \qquad (23a)$$
$$\times\ {}_2F_1[i\frac{\eta}{2} - i\beta + \frac{1}{2},\ i\frac{\eta}{2} + i\beta + \frac{1}{2};\ \frac{1}{2} + i\eta;\ -(\frac{v}{c})^2 e^{-\Gamma L}]/D$$

$$C_2 = \frac{-A(0)}{\sqrt{1+(v/c)^2}} (\frac{v}{c})^2\ {}_2F_1[-i\frac{\eta}{2} - i\beta + 1,\ -i\frac{\eta}{2} + i\beta + 1;\ \frac{3}{2} - i\eta;\ -(\frac{v}{c})^2 e^{-\Gamma L}]/D \qquad (23b)$$

$$C_3 = -A(0)\left(\frac{v\,(2+4i\eta)\,\sin\phi}{i\,c e^{i\phi}\sqrt{1+(v/c)^2}}\right) e^{(1-2i\eta)\Gamma L/2} \qquad (23c)$$
$$\times\ {}_2F_1[i\frac{\eta}{2} - i\beta + 1/2,\ i\frac{\eta}{2} + i\beta + \frac{1}{2};\ \frac{\eta}{2} + i\eta;\ -(\frac{v}{c})^2 e^{-\Gamma L}]/D$$

$$C_4 = A(0)\left(\frac{v\,(2+4i\eta)\,\sin\phi}{i\,c e^{i\phi}\sqrt{1+(v/c)^2}}\right) {}_2F_1[-i\frac{\eta}{2} - i\beta + 1,\ -i\frac{\eta}{2} + i\beta + 1;\ \frac{3}{2} - i\eta;\ -(\frac{v}{c})^2 e^{-\Gamma L}]/D \qquad (23d)$$

where the common denominator D is given by

$$D = 4\sin^2\phi\,(1+4\eta^2)\, e^{(1-2i\eta)\Gamma L/2}\ {}_2F_1[i\frac{\eta}{2} - i\beta + \frac{1}{2},\ i\frac{\eta}{2} + i\beta + \frac{1}{2};\ \frac{1}{2} + i\eta;\ -(\frac{v}{c})^2 e^{-\Gamma L}]$$
$$\times\ {}_2F_1[-i\frac{\eta}{2} - i\beta + \frac{1}{2},\ -i\frac{\eta}{2} + i\beta + \frac{1}{2};\ \frac{1}{2} - i\eta;\ -(\frac{v}{c})^2] \qquad (24)$$
$$-(\frac{v}{c})^2\ {}_2F_1[-i\frac{\eta}{2} - i\beta + 1,\ -i\frac{\eta}{2} + i\beta + 1;\ \frac{3}{2} - i\eta;\ -(\frac{v}{c})^2 e^{-\Gamma L}]\ {}_2F_1[i\frac{\eta}{2} - i\beta + 1,\ i\frac{\eta}{2} + i\beta + 1;\ \frac{3}{2} + i\eta;\ -(\frac{v}{c})^2]$$

the reflectivity is given by $R = |B(0)/A(0)|^2$. It is plotted in figure 3. for the case of equal intensity input beams (during the writing phase), for several values of the grating phase ϕ. In general, the reflectivity maximum occurs at a different frequency than that of the writing beams; it occurs at a frequency mismatch of $\Delta\beta = g/2\cos\phi$. The reflectivity plotted in figure 3 is symmetric about the line $\Delta\beta = 0$ when ϕ is reflected about $\pi/2$; for this reason we have only illustrated the reflectivity versus frequency mismatch for $0 \le \phi \le \pi/2$. We note that the grating apodization caused by intensity coupling for $\phi \neq 0$ or π leads to reduced sidelobes in the reflectivity, and lower overall reflectivity at large values of frequency mismatch. This is illustrated in figure 4. where the reflectivity of the $\phi = 0$ and $\phi = \pi/2$ cases are compared at large

values of mismatch.

We now consider how the previous equations are simplified under special conditions. For $\phi = \pi/2$ we note that the beam coupling consists purely of intensity coupling rather than phase coupling. This leads to a simpler form of the index grating (Equation 10.), however, little simplification of the final solutions occurs. Since the phase coupling is absent in this case, the reflectivity maximum of the grating occurs at the same frequency as that of the writing beams.

The case $\phi = 0$, is completely different. Here, there exists no intensity coupling while the phase coupling is maximum. Hence the magnitude of the index grating is a constant throughout the volume of the crystal. We obtain, in analogy to equation 10,

$$\Delta n = n_1 \frac{\sqrt{I_1(0)I_2(0)}}{I} e^{i g z} \tag{25}$$

The reflectivity is easily shown to be

$$R = \frac{\kappa^2 \mathrm{Sinh}^2 sL}{\kappa^2 \mathrm{Sinh}^2 sL + s^2} \tag{26}$$

where

$$\kappa = g \frac{\sqrt{I_1(0)I_2(0)}}{I} \tag{27a}$$

$$s = \sqrt{\kappa^2 - \delta^2/4} \tag{27b}$$

$$\delta = g - 2\Delta\beta \tag{27c}$$

Equation 26 has the simple form characteristic of Bragg reflection from a constant grating[8] except for the frequency shift in maximum reflectivity which here occurs at $\Delta\beta = g/2$ rather than $\Delta\beta = 0$.

A similar case occurs for arbitrary phase ϕ when c=0; that is, when the coupled beams are everywhere of equal intensity. Starting again from equations 4a and b we derive in analogy to equations 8 and 9 intensities and phases of the coupled beams

$$I_1(z) = I_2(z) = \frac{1}{2} v\, e^{-\Gamma z/2} = I_1(0)\, e^{-\Gamma z/2} \tag{28}$$

$$\psi_1(z) = -\psi_2(z) = \cos\phi\ g/2\ z \tag{29}$$

where v is as defined following equation 8a,b. From these we derive the index grating to be a constant magnitude

$$\Delta n(z) = \frac{n_1}{2} e^{i\, g \cos\phi\, z} \tag{30}$$

This grating is fixed in the material. The coupled mode equations describing reflection become

$$A'(z) = i \frac{g}{2} e^{i\phi} e^{i (g\cos\phi - 2\Delta\beta) z} B(z) \tag{31a}$$

$$B'(z) = -i \frac{g}{2} e^{-i\phi} e^{-i (g\cos\phi - 2\Delta\beta) z} A(z) \tag{31b}$$

these equations are readily solved to yield a reflectivity identical in form to that in the case $\phi = 0$ (Equation 26) with the modified definitions $\kappa = g/2$ and $\delta = g\cos\phi - 2\Delta\beta$.

Investigation, Lossy Case

When the loss in the material is considered, the equations become substantially more complicated. Analytic expressions are only obtained for dynamic holography, and only for ϕ=0. Reflectivities of the fixed holograms are calculated numerically. We start with the dynamic coupled mode equations as in equations 4a,b.

$$A'(z) = i\,g\,|B(z)|^2/I(z)\,e^{i\phi}A(z) - \alpha/2\,A(z) \quad (32a)$$

$$B'(z) = -i\,g\,|A(z)|^2/I(z)\,e^{-i\phi}B(z) + \alpha/2\,B(z) \quad (32b)$$

Performing the same transformation as in equation 5 we are led to the following equations for the phases and magnitudes of the coupled beams.

$$a'(z) = -\sin\phi\, g\,|b(z)|^2/I(z)\,a(z) - \alpha/2\,a(z) \quad (33a)$$

$$b'(z) = -\sin\phi\, g\,|a(z)|^2/I(z)\,b(z) + \alpha/2\,b(z) \quad (33b)$$

$$\psi_1'(z) = \cos\phi\, g\,|b(z)|^2/I(z) \quad (34a)$$

$$\psi_2'(z) = -\cos\phi\, g\,|a(z)|^2/I(z) \quad (34b)$$

Again, the special case $\phi=0$ yields considerably simplified formulas. In this special case, analytic solutions of equations 33 and 34 are obtained easily. They are

$$A(z) = A(0)\,e^{-\alpha z/2}\left[\frac{B(0)^2e^{2\alpha z}+A(0)^2}{B(0)^2+A(0)^2}\right]^{\frac{ig}{2\alpha}} \quad (35a)$$

$$B(z) = B(0)\,e^{+\alpha z/2}\left[\frac{B(0)^2+A(0)^2e^{-2\alpha z}}{B(0)^2+A(0)^2}\right]^{\frac{ig}{2\alpha}} \quad (35b)$$

Thus the index grating is given by

$$\Delta n(z) = n_1\frac{A(0)\,B(0)\,e^{igz}}{A(0)^2e^{-\alpha z}+B(0)^2e^{\alpha z}} \quad (36)$$

When this grating is fixed, we can formulate the coupled equations describing reflectivity in analogy to 11a,b, using equations 32a,b. These equations can be manipulated following identical steps as in the analysis up to equation 20a,b. In this case, however, instead of the Pöschl-Teller (Equation 20.), the second order equation obtained is a symmetric top equation[6,9]. We do not present its solution here, since it is useful only for $\phi=0$.

Alternatively, we have solved equations 32a and b numerically for arbitrary

photorefractive phase ϕ in order to obtain the index grating which is fixed in the material. This calculated index grating is then fitted to a high order polynomial (usually 9th order), and that polynomial approximation is then used in the reflectivity equations. In solving the dynamic equations we specify boundary conditions at z=0; i.e. A(0) and B(0). Then B(0) was iteratively modified to obtain the desired value for B(L), which is the physical input to the crystal. When the reflectivity was calculated, we used the standard procedure of fixing B(L) = 0 and A(L) = 1 and working backwards toward z=0. Finally, the reflectivity is normalized relative to the numerically computed A(0) (where $|A(0)| > 1$). The addition of a nonzero loss has two dramatic effects on the results. First, the reflectivity of the filter is now strongly nonreciprocal. Second, since energy is no longer conserved, the quantity $|A(z)|^2 - |B(z)|^2$ is no longer constant. In fact, the intensities can become equal at any arbitrary point within the volume of the crystal. Thus the index grating may have its maximum at any point in the volume of the crystal, rather than only at the entrance or exit facet.

In the following calculations we have used, as above, a coupling constant g=20/cm, a crystal length of L= 0.2cm, and we have assumed equal intensity inputs A(0) and B(L). The loss coefficient is taken to be $\alpha = 6/cm$. First the equations for the dynamically coupled beams A(z) and B(z) are computed from equations 32a and b. The results for various values of the grating phase ϕ are shown in figures 5a and b. The nonzero loss mostly affects the shape of B(z), incident from z = L. This occurs because the beam coupling and loss mechanisms are opposed. Thus B(z) has a minimum at the position where the material loss is balanced by the beam coupling. Also, the loss allows the two beams to have equal intensities at one point in the volume of the crystal. From equations 32 we determine that this condition is

allowed roughly when $g/2 \sin\phi < \alpha$. The index grating formed by the two beams (Figure 6.) illustrates this effect. For $\phi = 0$, it is clear that the index grating is maximum in the center of the crystal.

Next we calculate numerically the reflectivity from the index gratings of figure 6. Figure 7. shows the reflectivity for a beam incident on the z=0 side of the crystal, and figure 8. shows the reflectivity under the same conditions for a beam incident from z=L. Since the index grating is, in general, stronger near $z = 0$, the reflectivity is higher for a beam incident at $z = 0$. The difference between the two cases is most pronounced when the grating phase ϕ is near $\pi/2$. Also we point out that the behavior of the reflectivity as ϕ increases is more complex in the case of reflection from the $z = 0$ side. This occurs because the index grating near $z = 0$ (the most efficient region of reflection for a beam incident at $z = 0$) first increases, then decreases with increasing photorefractive phase ϕ. We can see how this effect arises by an inspection of the shape of B(z) in figure 5b.

In summary; we describe an analytic solution for the frequency response of interference filters written with the photorefractive effect. We allow for an arbitrary photorefractive grating phase ϕ. In addition we have presented numerical solutions of the identical procedure with a nonzero optical absorption in the material. A number of aspects of the interplay between the intensity and phase coupling due to ϕ are discussed.

The authors express their gratitude to the Army Research Office (Durham), the Air Force Office of Scientific Research, and the Advanced Research Projects Agency (DARPA) for supporting this work.

References

[1] G. Rakuljic, A. Yariv, and V. Leyva, "High Resolution Volume Holography Using Orthogonal Data Storage," Photorefractive Materials, Effects, and Devices Conference of OSA, July 29-31, 1991, Beverley, MA, paper MD-3

[2] G. Rakuljic, V. Leyva, and A. Yariv, "Optical Data Storage Using Orthogonal Wavelength Multiplexed Volume Holograms," to be published Oct 15 in Opt. Lett.

[3] V. Leyva, G. Rakuljic, and A. Yariv, "Volume Holography Using Orthogonal Data Storage Approach," OSA annual meeting Nov 3-8, 1991, San Jose, CA, paper FU-7

[4] G. Rakuljic, et. al. , "Comparison of Angle and Wavelength Multiplexing in Holographic Data Storage (invited paper)," OSA annual meeting Sept 20-25, 1992, Albequerque, NM, paper WE-2

[5] J. O. White, et. al. , *Photorefractive Materials and their Applications II*, chap. 4, eds. P. Günther and J. P. Huignard (Springer-Verlag, Berlin, 1989)

[6] A. O. Barut, A. Inomata, and R. Wilson, "Algebraic treatment of second Pöschl-Teller, Morse-Roesn, and Eckart equations," J. Phys. A: Math. Gen. **20**, 4083-4090 (1987)

[7] L. Infeld, T. E. Hull, "The Factorization Method," Rev Mod Phys **23**, 21-68 (1951)

[8] A. Yariv, *Optical Electronics* 4th ed. , (Saunders College Publishing, Philadelphia, 1991), p. 496

[9] D. Zwillinger, *Handbook of Differential Equations*, (Academic Press, New York, 1989)

Figure Captions

Figure 1. The effect of the photorefractive grating phase ϕ on the intensity coupling of two equal intensity input beams. For $\phi = 0$, the intensity coupling is zero, and the beams are purely phase coupled. As ϕ deviates from zero, the beams are coupled more and more strongly near the entrance face of the crystal. The coupling constant is $g = 20/cm$, and the crystal length is $L = 0.2cm$.

Figure 2. The magnitude of the index grating formed by the intensity coupled beams from figure 1. For $\phi = 0$, the index grating is constant, and as ϕ increases, the index grating is more strongly apodized with its maximum at the entrance face of the crystal.

Figure 3. The reflectivity from the fixed index gratings of figure 2. The reflectivity maximum occurs at a frequency mismatch given by $\Delta\beta = g/2\cos\phi$. The overall reflectivity as well as the sidelobes are reduced by the grating apodization for $\phi > 0$.

Figure 4. The reflectivity from the fixed index gratings for $\phi = 0$ and $\phi = \pi/2$ at large values of frequency mismatch. The $\phi = \pi/2$ grating reflectivity has reduced sidelobes whose peaks are approximately 10dB lower than the $\phi = 0$ case.

Figure 5a. The intensity of beam 1 incident at z=0 for various values of ϕ, for a loss constant of $\alpha = 6/cm$, and for equal intensity inputs. The coupling constant is $g = 20/cm$, and the crystal length is $L = 0.2cm$. **5b.** The intensity of beam 2 incident at z=L under identical conditions as figure 5a.

Figure 6. The index grating formed in the crystal by the coupled beams in figure 5. The effect of the loss is to eliminate the "no crossing" rule for the two beam intensities. Thus when $g/2 \sin\phi \leq \sim \alpha$ the intensities can be equal within the volume of the crystal. This leads to a maximum in the magnitude of the index grating located away from the edge of the crystal.

Figure 7. Reflectivity for the case $\alpha = 6/\text{cm}$, versus frequency mismatch, for a beam incident at z=0 on the index gratings of figure 6. The behavior is complex because the magnitude of the index grating near z=0 (the most efficient region of reflection) first increases then decreases with increasing photorefractive grating phase ϕ.

Figure 8. Reflectivity for the case $\alpha = 6/\text{cm}$, versus frequency mismatch, for a beam incident at z=L on the index gratings of figure 6. Note the strong non-reciprocity compared with figure 7. The behavior for this case is simpler than that of figure 7. because the magnitude of the index grating near z=L (the most efficient region of reflection) decreases monotonically with increasing photorefractive grating phase ϕ.

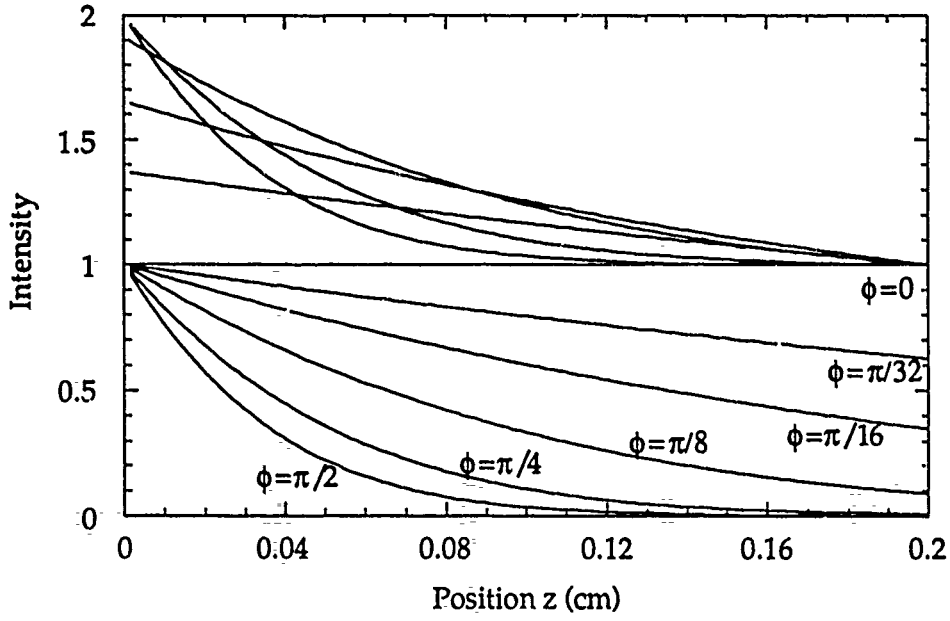
2
1.5
1
0.5
0
Intensity
0
0.04
0.08
0.12
0.16
0.2
Position z (cm)
ϕ=0
ϕ=π/32
ϕ=π/16
ϕ=π/8
ϕ=π/4
ϕ=π/2

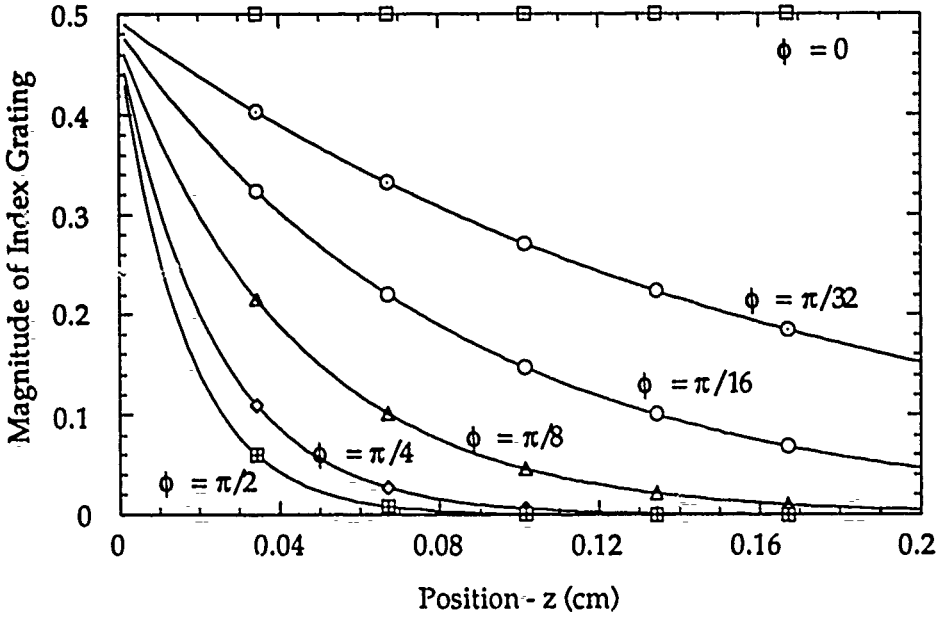
0.5
0.4
0.3
0.2
0.1
0
Magnitude of Index Grating
0
0.04
0.08
0.12
0.16
0.2
Position - z (cm)
ϕ = 0
ϕ = π/32
ϕ = π/16
ϕ = π/8
ϕ = π/4
ϕ = π/2

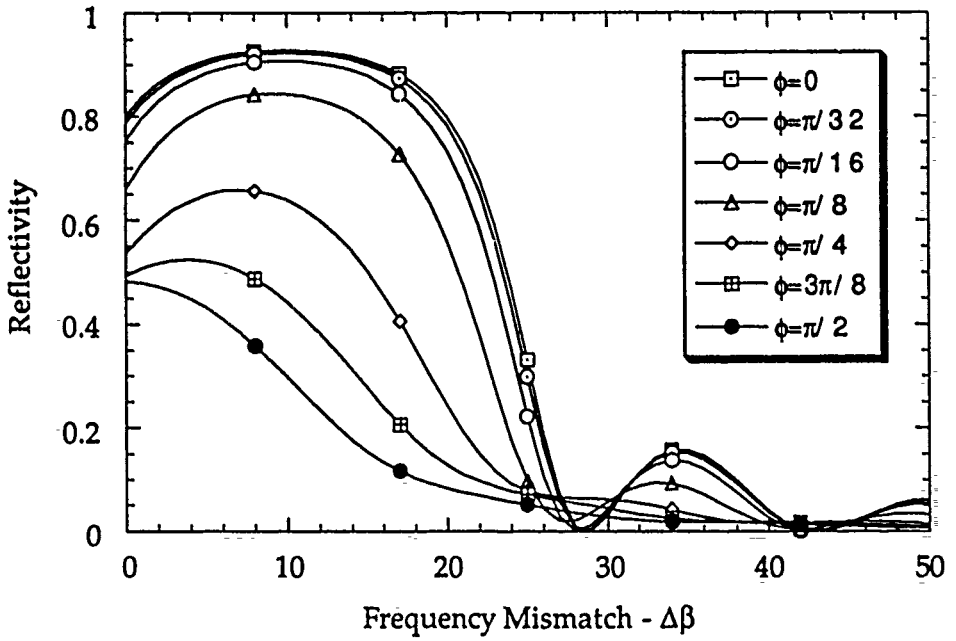
Reflectivity
1
0.8
0.6
0.4
0.2
0
0
10
20
30
40
50
Frequency Mismatch - Δβ
ϕ=0
ϕ=π/32
ϕ=π/16
ϕ=π/8
ϕ=π/4
ϕ=3π/8
ϕ=π/2

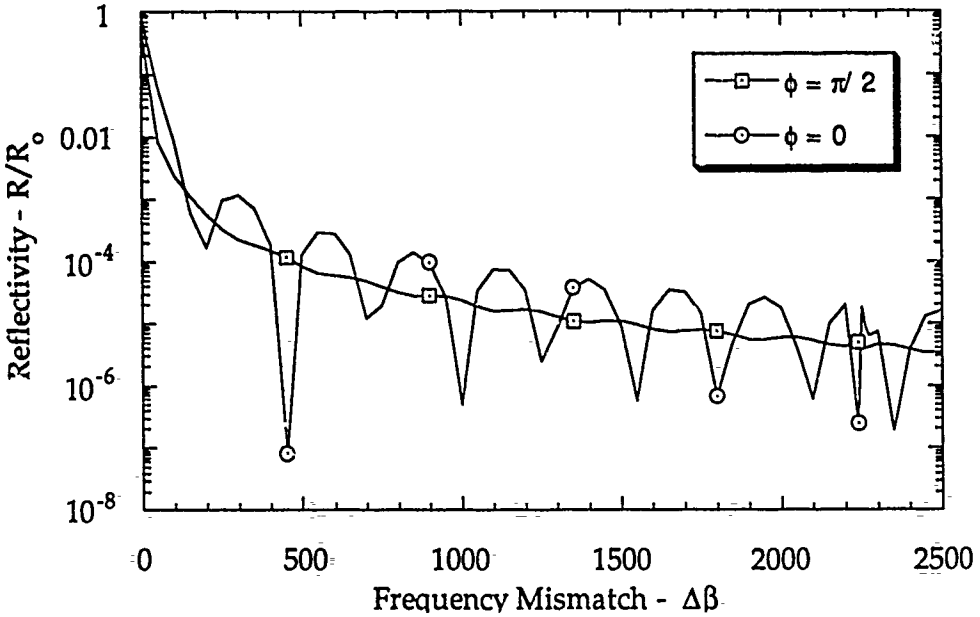
1
0.01
10^{-4}
10^{-6}
10^{-8}
Reflectivity - R/R_o
0
500
1000
1500
2000
2500
Frequency Mismatch - $\Delta\beta$
$\phi = \pi/2$
$\phi = 0$

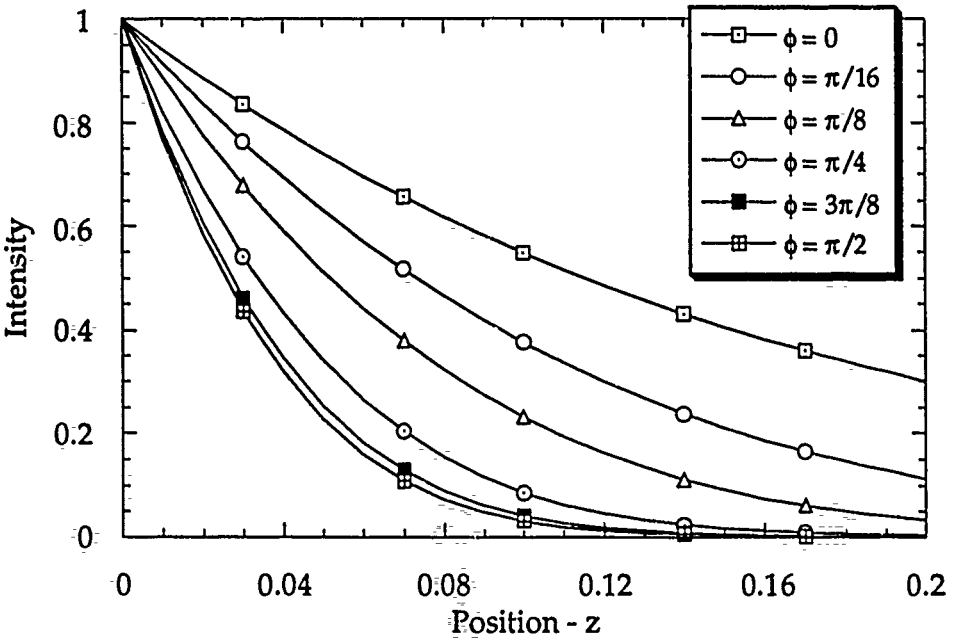
1
0.8
0.6
0.4
0.2
0
Intensity
0
0.04
0.08
0.12
0.16
0.2
Position - z
ϕ = 0
ϕ = π/16
ϕ = π/8
ϕ = π/4
ϕ = 3π/8
ϕ = π/2

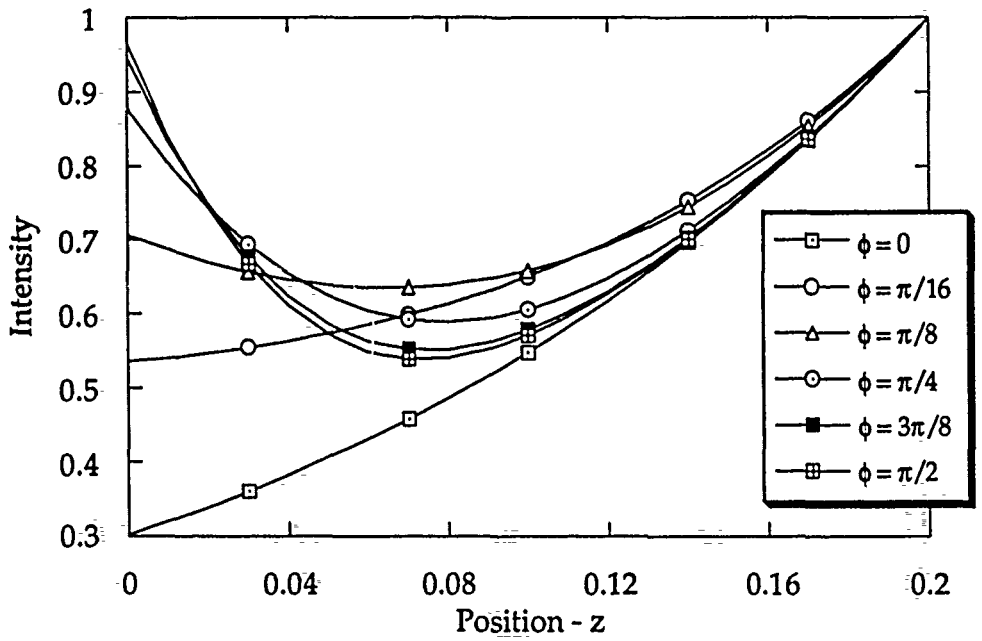
1
0.9
0.8
0.7
0.6
0.5
0.4
0.3
Intensity
0
0.04
0.08
0.12
0.16
0.2
Position - z
φ = 0
φ = π/16
φ = π/8
φ = π/4
φ = 3π/8
φ = π/2

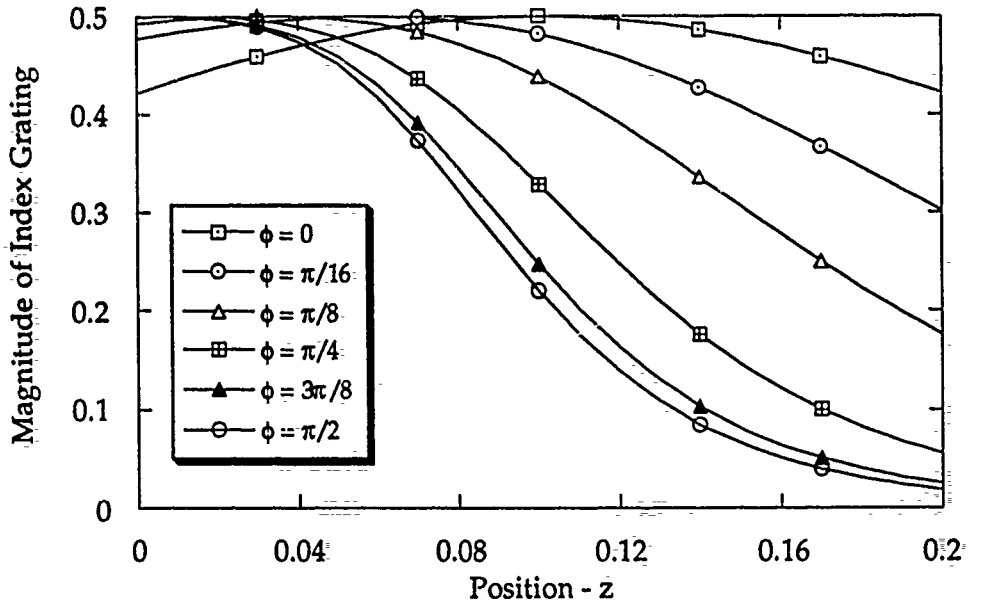
Magnitude of Index Grating
0.5
0.4
0.3
0.2
0.1
0
0
0.04
0.08
0.12
0.16
0.2
Position - z
φ = 0
φ = π/16
φ = π/8
φ = π/4
φ = 3π/8
φ = π/2

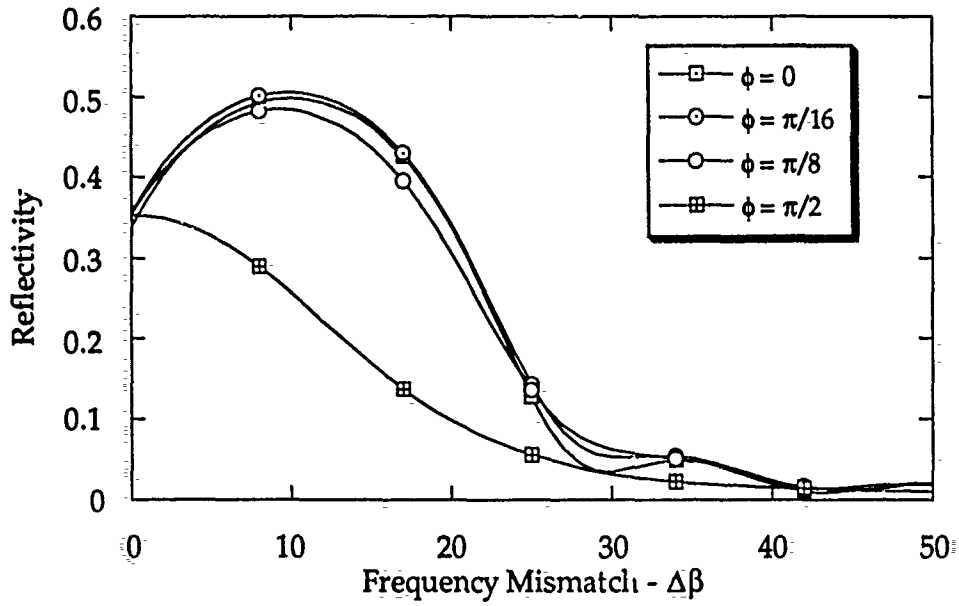
0.6
0.5
0.4
0.3
0.2
0.1
0
Reflectivity
0
10
20
30
40
50
Frequency Mismatch - Δβ
ϕ = 0
ϕ = π/16
ϕ = π/8
ϕ = π/2

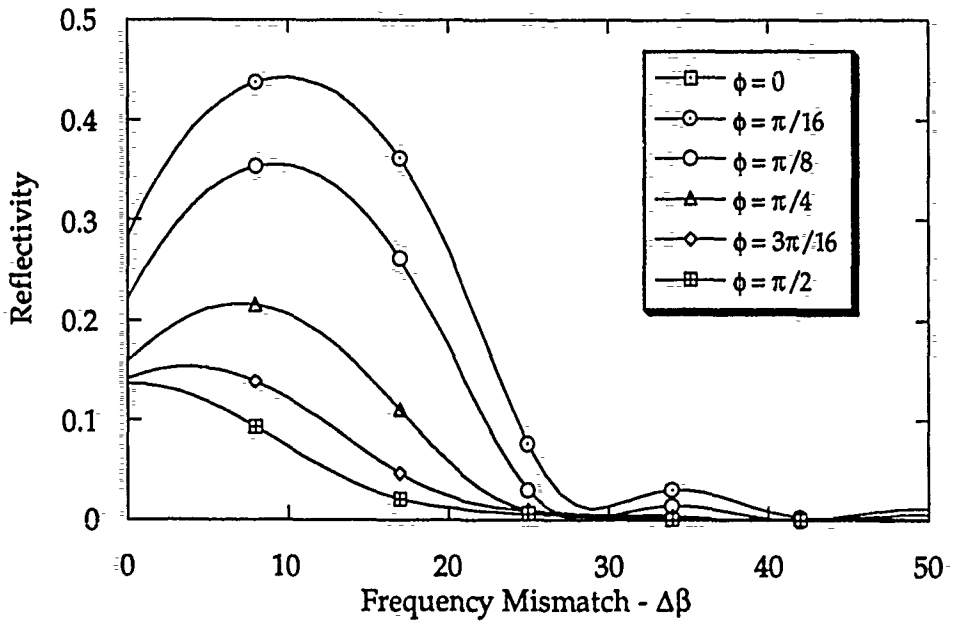
0.5
0.4
0.3
0.2
0.1
0
Reflectivity
0
10
20
30
40
50
Frequency Mismatch - Δβ
ϕ = 0
ϕ = π/16
ϕ = π/8
ϕ = π/4
ϕ = 3π/16
ϕ = π/2

Vibration Detection Using Dynamic Photorefractive Gratings in KTN/KLTN Crystals

Rudolf Hofmeister and Amnon Yariv
California Institute of Technology
Pasadena, CA 91125

Abstract

We demonstrate a sensitive, all-optical, self aligning holographic microphone/vibration sensor utilizing the zero external electric field photorefractive (Zefpr) effect. The device relies on the unique phase relationship, $\phi=0$, between a spatially periodic intensity standing wave and the resultant index grating created with the Zefpr effect. Under this zero phase condition, the transmitted intensity of interfering beams in a two beam coupling geometry varies linearly with displacement of either the index grating or one of the interfering beams. In this way, vibrations are sensed remotely without any electrical signals in the vicinity of the sensor. The sensitivity of the microphone was determined as a noise equivalent power of 15dB sound pressure level relative to 0.0002μbar across the range 1.6 - 15.5kHz.

Introduction

All-optical sensors have received considerable attention recently[1] for use in applications where electrical signals cannot be used or are impractical. These include aqueous, explosive, corrosive, and electromagnetically sensitive environments. Traditionally, intensity modulating sensors have been preferred over interferometric methods[2] because of their relative ease of alignment. Unfortunately, even these techniques require precise fiber positioning in order to gain sensitivity[2]. Thus they are not robust. We have been able to develop an interferometric vibration detector and microphone which overcomes the alignment and stability problems of conventional methods. The mechanism for the operation of these devices is the recently reported Zero External Field Photorefractive (Zefpr) effect in paraelectric KTN and KLTN crystals.

The Zero External Field PhotoRefractive (Zefpr) effect was first noticed by us[3,4] in paraelectric KTN and KLTN crystals. These materials lack a linear electrooptic coefficient above their phase transition temperature. Instead, the Zefpr effect has been attributed to the presence of a growth induced strain[5,6]. Recently, we have developed a method of producing KTNs and KLTNs with high niobium concentrations of high optical quality, and in these crystals the effect is pronounced. Under certain conditions of crystal preparation we have been able to produce Zefpr index gratings with $\Delta n = 1.7 \times 10^{-5}$, and diffraction efficiencies of over 20% in a 4.15mm thick sample using 488nm argon laser beams.

In the KTN and KLTN crystals which displayed a strong Zefpr effect, the

photorefractive dopant was copper, which is stable as either Cu^{1+} or Cu^{2+}. The Cu^{2+} ion is known to cause large Jahn-Teller (J-T) distortions, especially in octahedral symmetry. The Cu^{1+} ion, by contrast, has no tendency to distort[7]. Illumination of the crystal by the periodic intensity pattern of the optical field leads to a mimicking spatially periodic Cu^{2+}/Cu^{1+} ratio due to excitation of electrons from Cu^{1+} and trapping by Cu^{2+}. This, as explained above, gives rise to a spatially periodic distortion. Since the copper concentration is relatively small in the KLTNs we do not expect a cooperative ordering of the distortions; rather, their orientation should be random. But when a macroscopic (growth induced) strain is present, as is the case in the crystals studied[5], distortions will orient preferentially in order to minimize that strain. The result is a spatial modulation of the strain field in phase with the intensity which leads to a corresponding modulation of the index of refraction (index grating) via the photoelastic effect. In the absence of a coordinating macroscopic strain, the Zefpr effect is weaker but remains, in general, nonzero.

Since the index grating is modulated by the local Cu^{2+} concentration, we expect it to be in phase with the intensity ($\phi = 0$) so that no two beam coupling (power exchange between the two writing beams) will occur. When either the phase of the index grating or of the interfering beams is modulated with $\alpha \ll \pi/2$, however, a power exchange, proportional to α, takes place between the two beams. If the vibration frequency is much higher than the inverse of the grating rewrite time, the vibration will not erase the grating. Optical fibers can be used to deliver the interfering light beams to and collect the transmitted beams from a Zefpr crystal. In this way, vibrations can be sensed remotely without any electrical signals in the vicinity of the sensor. In addition, since the detecting element is a holographic

grating which is continually rewritten, the device is self-aligning ; any change in the average position of the crystal, or the elements determining the beams' phases will be compensated by a buildup of a new grating with the appropriate $\phi=0$. The device is thus resistant to mechanical shocks. In the following paragraphs we describe the performance of the Zefpr microphone. The detection characteristics including output linearity are discussed.

The setup of the fiber microphone reported on here is illustrated in figure 1. A single mode fiber was used to deliver the 488nm light to the device. The emerging beam was collimated and split by a 90^0 prism. This method of beamsplitting was chosen over that using a fiber coupler, because couplers at this wavelength are expensive and problematic. One beam was reflected off a mirror, and the other off a membrane. The equal intensity beams interfered in the volume of the crystal , and the outputs of the two beams were detected differentially. Most of the light was blocked in order not to saturate the detectors. Since the beams are not deflected, but only intensity modulated, we conclude that it will be relatively easy to couple the output light into multimode fibers.

The membrane was a uniformly stretched circular film of reflective mylar. Since both sides were open to the air, it operated as a pressure gradient sensor, with resultant poor low frequency response. The first resonance of the membrane was at 900Hz. The usable range of operation was from 1.2 - 25kHz (the limit of the spectrum analyzer).

The detector outputs were processed with an audio spectrum analyzer. The performance of the microphone was evaluated for both single ended and differential detection. Figure 2a shows the output of a single detector with a 58dB sound pressure level (SPL relative to 0.0002μbar) signal at 4.9kHz incident on the

microphone. The background noise floor is also plotted. From the figure, we measure a noise equivalent power (NEP) of 38dB. Figure 2b shows the same incident signal detected differentially. The compensation of intensity fluctuations with differential detection lowers the noise floor by 26dB, leading to an NEP of 12dB SPL. Between the range of 1.6 - 15.5kHz we determined the NEP ≤ 15dB.

When two beams $I_1(0)$ and $I_2(0)$ are symmetrically incident (Figure 3) on a Zefpr ($\phi = 0$) material it can be shown that the resultant index grating is given by

$$n(r,t) = n_0 + \frac{n_1}{2I_0}|A_1(0)||A_2(0)|\, e^{i\Delta z} e^{-i(k_1-k_2)z} + c.c. \qquad (1)$$

where $\Delta = (g/I_o)(I_2(0) - I_1(0))$, $g = \pi n_1/\lambda$, and n_1 is the index modulation for $I_2(0) = I_1(0)$. $A_i(0)$ are the complex amplitudes of the input beams. If this index grating is considered fixed in the crystal and one beam is phase shifted by $\alpha = \alpha_1 \sin \omega t$, where $\alpha_1 \ll \pi/2$ and $1/\omega \ll \tau_{write}$ then the coupled mode equations can be solved to yield

$$I_1(z) = I_1(0)\left(1 - \frac{\kappa^2}{s^2}\sin^2(sz)\right) + I_2(0)\frac{\kappa^2}{s^2}\sin^2(sz) - \frac{\kappa}{s}|A_1(0)||A_2(0)|\sin(2sz)\sin(\alpha) - \frac{\kappa\Delta}{s^2}|A_1(0)||A_2(0)|\sin^2(sz)\cos(\alpha) \qquad (2a)$$

$$I_2(z) = I_2(0)\left(1 - \frac{\kappa^2}{s^2}\sin^2(sz)\right) + I_1(0)\frac{\kappa^2}{s^2}\sin^2(sz) + \frac{\kappa}{s}|A_1(0)||A_2(0)|\sin(2sz)\sin(\alpha) + \frac{\kappa\Delta}{s^2}|A_1(0)||A_2(0)|\sin^2(sz)\cos(\alpha) \qquad (2b)$$

where $s^2 = \kappa^2 + \Delta^2/4$, and $\kappa = g\, A_1 A_2^*/I_o$. In figure 4a the output is plotted for $\alpha_1 = 0.15$rad, for $A_2(0) = A_1(0)$, for the cases gL= 0.5 and 1.0.

The same calculation can be performed for a conventional photorefractive material ($\phi = \pi/2$). The result is

$$I_1(z) = I_1(0)\,[\cos^2(\gamma-\delta) + \zeta^2\sin^2(\gamma-\delta) + \zeta\sin(2(\gamma-\delta))\cos(\alpha)] \qquad (3a)$$

$$I_2(z) = I_1(0)\,[\zeta^2\cos^2(\gamma-\delta) + \sin^2(\gamma-\delta) - \zeta\sin(2(\gamma-\delta))\cos(\alpha)] \qquad (3b)$$

where $\zeta^2 = I_2(0)/I_1(0)$, $\gamma = \mathrm{Tan}^{-1}[\zeta e^{\kappa z}]$, and $\delta = \mathrm{Tan}^{-1}[\zeta]$. Figure 4b plots the output signal for the same experimental conditions as in figure 4a. The signal amplitude is much weaker than in the $\phi = 0$ case and is at twice the modulating frequency. The details of these calculations will be presented elsewhere. From these figures it is clear that only a material with zero phase gratings is sensitive to small phase fluctuations, the sensitivity of the conventional photorefractive decreasing with increasing coupling constant. In addition, the zero phase grating yields a linear response whereas the conventional photorefractive gives the second harmonic. Thus only a zero phase material is suitable as an all-optical vibration sensor (though a conventional material can be made to approximate the zero phase condition by appiying an electric field or frequency shifting one of the beams).

We have demonstrated a sensitive all-optical microphone/vibration detector utilizing the Zefpr effect. Investigation of the two-beam coupled equations reveal that only a zero phase photorefractive material such as Zefpr materials are suitable for vibration detection and, in particular, for linear vibration detection. R. Hofmeister would like to thank Y. Shevy for valuable discussions and suggestions on the experimental procedure. This research was performed with the support of the Army Research Office grant (R. Guenther), and the Air Force Office of Scientific Research (H. Schlossberg).

References

[1] P. M. Tracey, IEEE-Ind-Ap **27**, 96 (1991)

[2] D. Garthe, Sensors and Actuators A, **25**, 341 (1991)

[3] A. Agranat, V. Leyva, and A. Yariv, Opt. Letters **14** 1017 (1989)

[4] A. Agranat, R. Hofmeister, and A. Yariv Technical Digest on Photorefractive Materials, Effects, and Devices, 1991 (Optical Society of America, Washington DC, 1991) Vol **14** 6

[5] R. Hofmeister, A. Agranat, and A. Yariv, Opt. Letters **17**, 713 (1992)

[6] R. Hofmeister, A. Yariv, S. Yagi, A. Agranat, submitted for publication

[7] A. F. Wells, Structural Inorganic Chemistry 4th Ed. , Clarendon Press, Oxford (1975)

Figure Captions

Figure 1. The setup of the Zefpr microphone. A prism **P** is used to split the incident beam. Reflections off the mirror **M** and the membrane interfere within the Zefpr crystal **Xtl**. Vibrations of the membrane cause two-beam coupling fluctuations which are detected (**Det**) differentially.

Figure 2a. The output of one detector with a 58dB signal at 4.9kHz incident on the microphone. The lower trace is the noise floor without the signal. The NEP is 38dB. **2b.** The differential output of both detectors under the same experimental conditions. Compensation of intensity fluctuations lowers the noise floor 26 dB yielding NEP = 12dB.

Figure 3. Schematic of the two-beam coupling geometry used.

Figure 4a. Intensity modulation of a Zefpr material in the geometry of figure 3 for a sinusoidal input phase modulation of 0.15rad. The output approximates a sine wave at the same frequency (fitted curves) even for large amplitudes. **4b.** Intensity modulation of a conventional photorefractive under the same conditions. The output is a weak modulation at twice the input frequency.

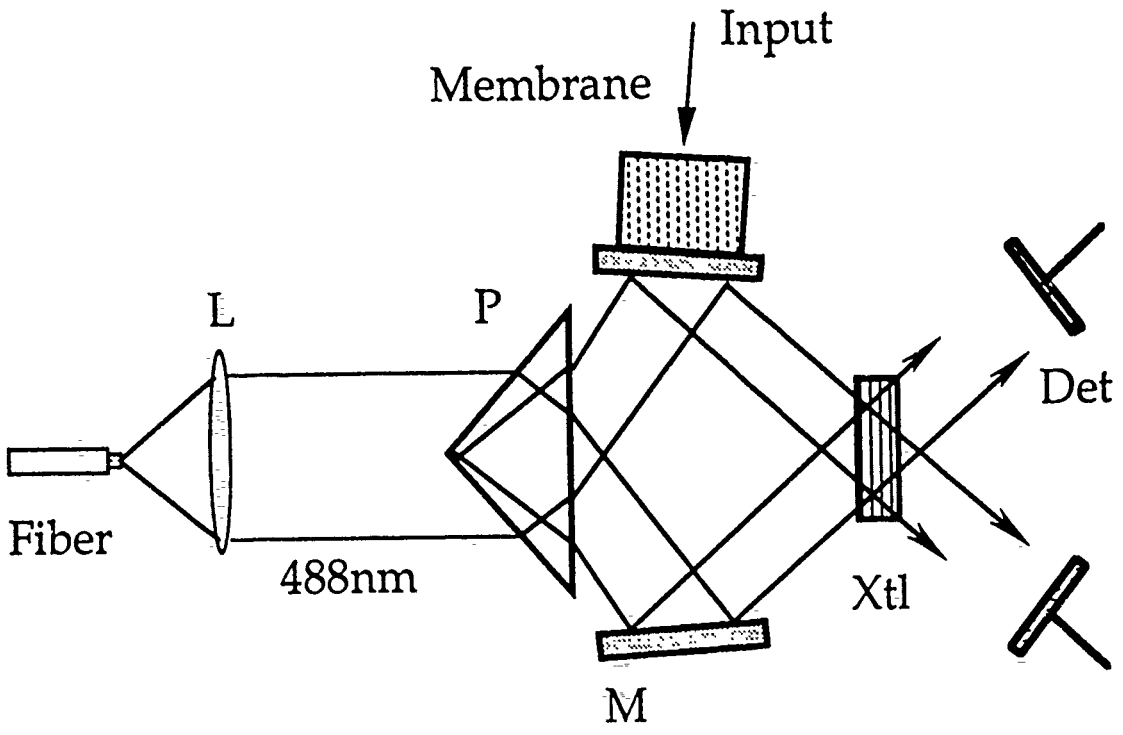
Input
Membrane
L
P
Det
Fiber
488nm
Xtl
M

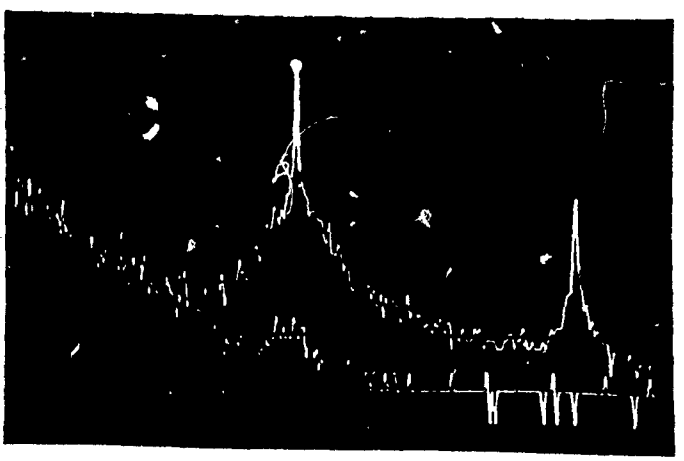

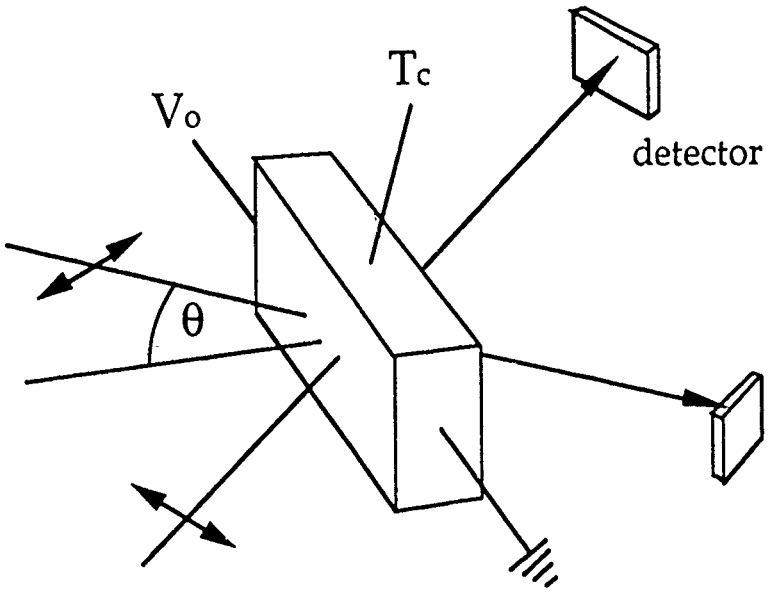
Tc
Vo
detector
θ

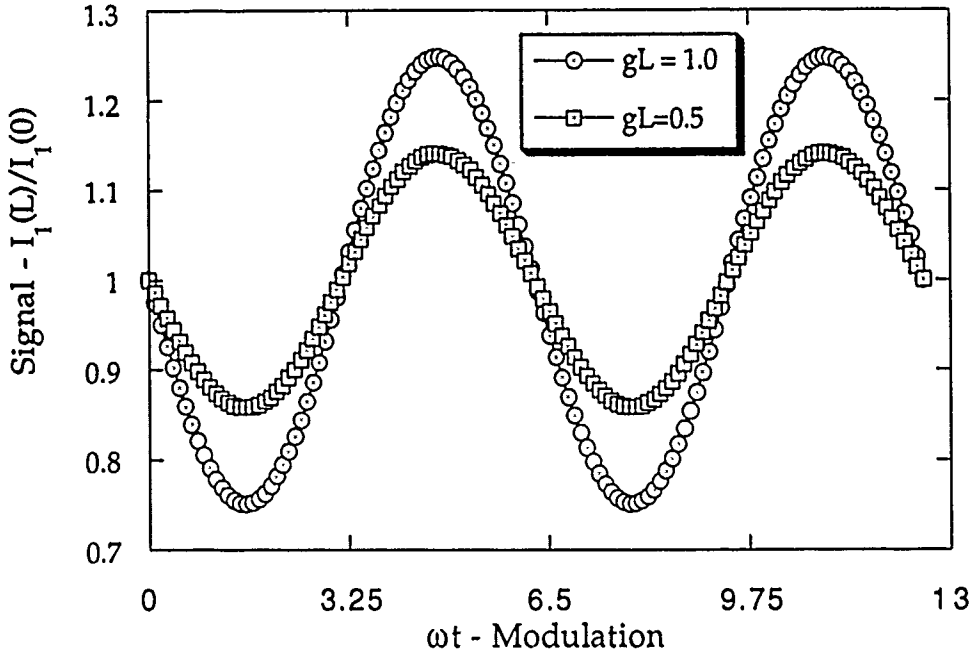
1.3
1.2
1.1
1
0.9
0.8
0.7
Signal - $I_1(L)/I_1(0)$
gL = 1.0
gL=0.5
0
3.25
6.5
9.75
13
ωt - Modulation

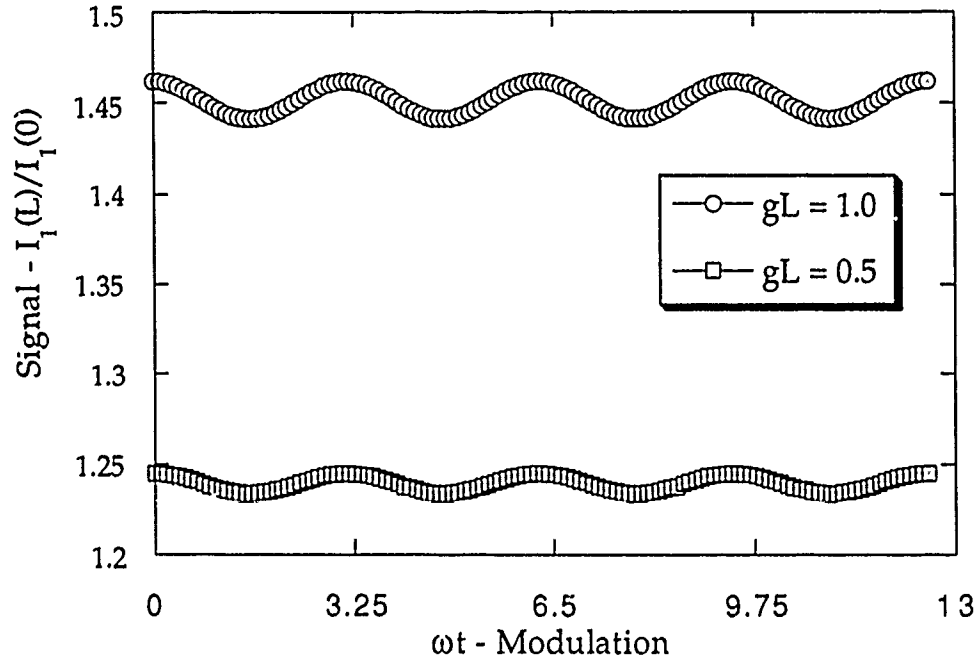
1.5
1.45
1.4
1.35
1.3
1.25
1.2
Signal - $I_1(L)/I_1(0)$
gL = 1.0
gL = 0.5
0
3.25
6.5
9.75
13
ωt - Modulation

APPENDIX C

Simple Methods of Measuring the Photorefractive Phase Shift and Coupling Constant

Rudolf Hofmeister, Amnon Yariv, Anthony Kewitsch, and Shogo Yagi*
California Institute of Technology
Pasadena, CA 91125

* permanent address NTT Interdisciplinary Research Laboratories
Ibaraki, Japan

Abstract

We report measurements of the photorefractive phase shift and coupling constant of several photorefractive materials using three independent methods. We solve the problem of beam coupling in a material with a dynamically written grating for arbitrary input beams. The diffraction off the grating is calculated as a special case. These solutions are used to determine the beam coupling as a function of the photorefractive phase ϕ and coupling constant g when one beam is either sinusoidally phase modulated or ramped in phase. Experimental results are obtained for $LiNbO_3$ and $BaTiO_3$, and for paraelectric KLTN as a function of applied electric field.

Introduction

The photorefractive grating phase ϕ and the coupling constant g are the two material parameters which describe the interaction of two or more coherent beams in a photorefractive material. Yet the exact determination of these parameters has received little attention to date. Most published reports describe approximate methods of phase determination[1, 2, 3, 4]. Here we report an exact solution of the coupled equations describing the evolution of two arbitrary beams incident at the Bragg angle on a dynamically written photorefractive grating. The incident beams need not possess the same phase nor the same intensity as the beams which wrote the grating. In our analysis, all the beams are of the same frequency.

Two coherent beams are symmetrically incident on a photorefractive crystal. They induce a spatially periodic space charge field E_{sc} which is phase shifted with respect to the intensity interference pattern by the photorefractive phase ϕ. A dynamically written refractive index grating is the result. The writing beams are then replaced with two beams with arbitrary intensity and phase and of the same frequency incident along the same directions as the initial beams i. e. , at the Bragg angles. We calculate the instantaneous beam coupling experienced by these new beams off the dynamically written grating which for the short initial period, is considered fixed. We ignore the time dependent formation of dynamic gratings written by the new beams.

We start by calculating the two beam coupling of two incident copropagating beams with amplitudes A(z) and B(z) in a photorefractive material (Figure 1). The well known coupled beam equations are[5]

$$A'(z)\cos\beta = \frac{i\pi\Delta n}{\lambda} e^{i\phi} B(z) - \frac{\alpha}{2} A(z) \quad (1a)$$

$$B'(z)\cos\beta = \frac{i\pi\Delta n^*}{\lambda} e^{-i\phi} A(z) - \frac{\alpha}{2} B(z) \quad (1b)$$

where λ is the wavelength of the interfering beams, α the optical absorption, and β the half-angle of beam intersection inside the material. The index of refraction is

$$n(z) = n_0 + \frac{1}{2}\left(\Delta n(z) e^{i\phi} e^{iKz} + c.c.\right) \quad (2)$$

Here ϕ is the photorefractive phase between the optical intensity grating and the induced index grating; $K = 2k\sin\beta$ is the grating wavevector . Since the index grating is formed dynamically by the writing beams we have

$$\Delta n(z) = n_1 A(z)\, B^*(z)/I(z) \quad (3)$$

where I(z) is the total intensity, and n_1 is the peak-to-peak amplitude of the index grating when A(z) = B(z). The intensities of the beams of equations 1a,b can be solved to yield[5]

$$I_1(z) = e^{-\alpha L} \frac{I_2 (I_1 + I_2)}{I_1 + I_2 e^{+\Gamma z}} \quad (4a)$$

$$I_2(z) = e^{-\alpha L} \frac{I_1 (I_1 + I_2)}{I_1 e^{-\Gamma z} + I_2} \quad (4b)$$

where $A(z) = [I_1(z)]^{1/2}\exp[i\zeta_1]$ and $B(z) = [I_2(z)]^{1/2}\exp[i\zeta_2]$, $\Gamma = 2g\sin\phi$, and $g = \pi n_1/\lambda$ is the material coupling constant. L is the effective thickness of the crystal: $L = d/\cos\beta$. We have defined $I_1 = I_1(0)$ and $I_2 = I_2(0)$. The phases of the two beams are given by

$$\zeta_1(z) = \frac{1}{2}\cot\phi \ln[I_1 + I_2 e^{+\Gamma z}] \quad (5a)$$

$$\zeta_2(z) = -g\cos\phi\, z - \frac{1}{2}\cot\phi \ln[I_1 + I_2 e^{+\Gamma z}] \quad (5b)$$

The index grating in the material follows from equations 2, 3, 4, and 5 and is given

by

$$\Delta n = n_1\sqrt{I_1 I_2}\left(I_1 e^{-\Gamma z/2} + I_2 e^{+\Gamma z/2}\right)^{i\cot\phi - 1} \qquad (6)$$

We calculate the beam coupling of a new set of Bragg matched beams $T(0) = [P_1]^{1/2}\exp[i\psi_1]$ and $V(0) = [P_2]^{1/2}\exp[i\psi_2]$ off this index grating. In analogy to equations 1a b we write the coupled mode equations

$$T'(z)\cos\beta = i\,g\sqrt{I_1 I_2}\, e^{+i(\phi+\theta)}\left(I_1 e^{-\Gamma z/2} + I_2 e^{+\Gamma z/2}\right)^{+i\cot\phi - 1} V(z) - \frac{\alpha}{2}T(z) \qquad (7a)$$

$$V'(z)\cos\beta = i\,g\sqrt{I_1 I_2}\, e^{-i(\phi+\theta)}\left(I_1 e^{-\Gamma z/2} + I_2 e^{+\Gamma z/2}\right)^{-i\cot\phi - 1} T(z) - \frac{\alpha}{2}V(z) \qquad (7b)$$

where $\theta = \zeta_1(0) - \zeta_2(0) - \psi_1(0) + \psi_2(0)$ is the phase difference between the intensity pattern of the beams which wrote the grating and that of T(0) and V(0). I_1 and I_2, are the intensities of the writing beams. Equations 7a, b ignore the new dynamic grating which is written by beams T(z) and V(z). This neglect is justified only for a short time, which however is amply long ($\geq$ 1 sec) to obtain the necessary data.

It is readily verified that equations 7a and 7b are satisfied by solutions of the form

$$T(z)\, e^{\alpha L/2} = C_1\left(I_2 + I_1 e^{-\Gamma z}\right)^{+i\eta - 1/2} + C_2\left(I_2 e^{+\Gamma z} + I_1\right)^{+i\eta - 1/2} \qquad (8a)$$

$$V(z)\, e^{\alpha L/2} = C_3\left(I_2 + I_1 e^{-\Gamma z}\right)^{-i\eta - 1/2} + C_4\left(I_2 e^{+\Gamma z} + I_1\right)^{-i\eta - 1/2} \qquad (8b)$$

where $\eta = \cot\phi/2$, and C_j are constants which are determined by the coupled equations and the boundary conditions.

We solve the coefficients C_j for two special cases. The first is the case where one or two of the reading beams are phase shifted relative to recording beams but their intensities are unchanged. This can be accomplished in practice by merely inserting a phase shift in the path of one of the recording beams. From equations 5a, b and the definition of θ in equations 7a and b we use the boundary conditions T(0)

$= I_1^{1/2}[I_1 + I_2]^{i\eta}$ and $V(0) = I_2^{1/2}[I_1 + I_2]^{-i\eta}$. We determine for this case

$$C_1 = \sqrt{I_1/(I_1+I_2)}\, I_2 \left(1 - e^{i\theta}\right) \quad (9a)$$
$$C_2 = \sqrt{I_1/(I_1+I_2)}\, \left(I_1 + I_2\, e^{i\theta}\right) \quad (9b)$$
$$C_3 = \sqrt{I_2/(I_1+I_2)}\, \left(I_2 + e^{-i\theta}\, I_1\right) \quad (9c)$$
$$C_4 = \sqrt{I_2/(I_1+I_2)}\, I_1 \left(1 - e^{-i\theta}\right) \quad (9d)$$

The output amplitudes T(L) and V(L) are thus determined. When $I_1 = I_2$ the transmitted intensities reduce to

$$P_1(z)/I_1 = 1 - \tanh[\Gamma z/2]\cos\theta - \frac{\sin(g\cos\phi\, z)}{\cosh[\Gamma z/2]}\sin\theta \quad (10a)$$

$$P_2(z)/I_1 = 1 + \tanh[\Gamma z/2]\cos\theta + \frac{\sin(g\cos\phi\, z)}{\cosh[\Gamma z/2]}\sin\theta \quad (10b)$$

The solutions for the case $I_1 << I_2$ also follow readily from equations 8 and 9, and agree with previously published results.[1] The results for the cases $\phi = 0$ and $\pi/2$ assume a simple form for arbitrary I_1 and I_2[6].

The other case considered is diffraction of a single incident beam off the grating. Here, we take V(0) = 0 and T(0) as before. In this case we obtain,

$$C_1 = \sqrt{I_1/(I_1+I_2)}\, I_2 \quad (11a)$$
$$C_2 = \sqrt{I_1/(I_1+I_2)}\, I_1 \quad (11b)$$
$$C_3 = \sqrt{I_2/(I_1+I_2)}\, I_1 = -C_4 \quad (11c,d)$$

Again, for the condition $I_1 = I_2$ the transmitted and diffracted intensities reduce to a simple form

$$P_1(z) = \frac{I_1}{2}\left(1 + \cos(g\cos\phi\, z)/\cosh(g\sin\phi\, z)\right) \quad (12a)$$

$$P_2(z) = \frac{I_1}{2}\left(1 - \cos(g\cos\phi\, z)/\cosh(g\sin\phi\, z)\right) \quad (12b)$$

Equations 4 and 12 can be used to determine g and ϕ in the material.

An alternate method of measuring g and ϕ follows when one of the interfering beams is phase shifted by

θ using a piezoelectrically driven mirror. The experimental configuration is as in figure 1. When the mirror is driven sinusoidally we have $\theta(t) = \theta_0 \sin(\omega t)$. If $\omega >> 1/\tau$, where τ is the writing time of the grating, and $\theta_0 << \pi/2$, and $I_1 = I_2$ then the powers of the transmitted beams at DC, ω, 2ω are related by

$$\left|\frac{P_{DC}}{P_{2\omega}}\right| = \frac{4}{\theta_0^2}\left(\coth[g \sin\phi\, z] \pm 1\right) \tag{13a}$$

$$\left|\frac{P_{\omega}}{P_{2\omega}}\right| = \frac{4}{\theta_0}\frac{\sin[g \cos\phi\, z]}{\sinh[g \sin\phi\, z]} \tag{13b}$$

where the powers are taken to be peak-to-peak values (Figure 2). The "+" in equation 13a refers to the beam which is amplified, and the "-" to the beam which is attenuated. If, instead of sinusoidal modulation, the piezoelectric mirror is ramped linearly in phase, then the phase positions during the ramp corresponding to the minimum and maximum of the transmitted intensities can be used to determine g and ϕ. In particular, the maximum of $P_2(z)$ from equation 10b occurs at

$$\theta_{max} = \tan^{-1}\left(\frac{\sin[g \cos\phi\, z]}{\sinh[g \sin\phi\, z]}\right) \tag{14a}$$

Equations (4), (12) and (13) constitute two independent methods of measuring g and ϕ. Equation (14) is a third method which can be used to verify the results obtained with the previous two methods. We used these methods to experimentally determine g and ϕ for an iron doped lithium niobate crystal, an iron doped barium titanate, and a paraelectric potassium lithium tantalate (KLTN) crystal doped with copper. The use of independent methods was instrumental in obtaining accurate data. Before the experimental setup was sufficiently isolated from air currents and vibration, each method yielded different results which, however, were remarkably consistent among themselves. Again the setup is illustrated in figure 1. All the experiments were performed at room temperature. The crystal dimensions were

3.82 x 5.49 x 2.34 mm^3 for the KLTN, 5.0 x 5.0 x 2.20 mm^3 for the $LiNbO_3$, and 5.0 x 5.0 x 5.23 mm^3 for the $BaTiO_3$, where the last dimension is the thickness of the sample. The KLTN was grown and prepared by us. The laser beams were at 488nm with polarization in the plane of their intersection. The c-axis of the samples was perpendicular to the bisector of the light beams in the plane of polarization. We used $K = 1.7x10^7/m$, and $\theta_o = .0613$rad at 10.6kHz for the sinusoidal phase modulation. The phase was not modulated during writing of the grating, although the effect of concurrent modulation and writing was almost negligible. When the phase was ramped through π radians to determine the phases of the intensity extrema, a similar procedure was used. Data was taken using a Stanford Research SR760 spectrum analyser and an HP7090A x-y plotter. The results for the samples tested are shown in table 1. The lithium niobate had $\phi = 0.41$ so that, despite a coupling constant of $g = 13.3/cm$, it showed weak beam coupling. For the barium titanate the phase was much closer to $\pi/2$ as is expected for a material with a weak photovoltaic effect. Paraelectric KLTN is forbidden from having a photorefractive response without an applied field, yet it does display the recently reported Zero Electric Field Photorefractive (Zefpr) effect of paraelectric crystals[7]. As predicted, the Zefpr gratings show $\phi = 0$ to within the accuracy of the experiment.

In addition, we determined the photorefractive parameters of the KLTN versus applied electric field. The photorefractive response of paraelectric KLTN is described by the quadratic electrooptic effect in conjunction with the Zefpr effect. The Zefpr gratings are unique in that they are always $\pi/2$ out of phase with the electrooptically induced index grating. In addition, the Zefpr index grating is proportional to the space charge field. We write

$\Delta n(z) = \Delta n_{EO} + \Delta n_{Zf}(z)$

$$\Delta n(z) = E_{sc}\left(\gamma E_0 \cos(Kz + \phi_E) + \gamma_{Zf} \sin(Kz + \phi_E)\right)$$
$$= E_{sc}\sqrt{(\gamma E_0)^2 + \gamma_{Zf}^2}\sin(Kz + \phi_E + \alpha) \qquad (15)$$

Here E_0 is the applied uniform electric field, E_{sc} the photorefractive space charge field, γ is given by[8] $\gamma = -n_o^3 g(\varepsilon\varepsilon_0)^2$, where n_o is the refractive index, g is the relevant quadratic electrooptic coefficient and $\varepsilon\varepsilon_0$ is the dielectric constant. γ_{Zf} is experimentally determined by the zero applied field diffraction, and ϕ_E is the phase between the intensity and electrooptic gratings. We have[5]

$$\phi_E = \tan^{-1}\left(\frac{E_0^2 + E_d^2 + E_d E_N}{E_0 + E_N}\right) \qquad (16)$$

where E_d and E_N are the photorefractive diffusion and maximum charge fields. The addition of the Zefpr grating modifies the net phase of the grating by $\alpha = \tan^{-1}(\gamma E_o/\gamma_{Zf})$, so that the photorefractive phase $\phi = \phi_E + \alpha$ is not equal to the phase between the intensity and the electrooptic grating. Finally, the coupling constant is given by $g = \pi\,[(\gamma E_o)^2 + \gamma_{Zf}^2]^{1/2} E_{sc,o}/\lambda$. Here $E_{sc,o}$ is the space charge field for unity modulation depth. The applied field dependence of the space charge field is given by[5]

$$E_{sc} = 2\frac{\sqrt{I_1 I_2}}{I}\,\frac{E_N(E_0 + iE_d)}{E_N + E_d - iE_0} \qquad (17)$$

The sample used had composition $K_{.99}L_{.01}T_{.71}N_{.29}:Cu_{.004}$. The acceptor concentration was determined with absorption data and grating spacing dependence of the space charge field to be $N_A = 1.5\text{x}10^{24}m^{-3}$. Capactive dielectric measurements yielded $\varepsilon = 12000$ at 24°C (the temperature of the experiment). The crystal was paraelectric above its phase transition at 15°C. Figures 3 and 4 show good agreement

between the experimentally determined values for g and ϕ versus applied field with the theory described above.

In summary, we have analyzed the problem of two-beam coupling and diffraction off a dynamic photorefractive grating written in the copropagating geometry. The solutions allow the determination of the coupling constant and phase of the photorefractive grating. These parameters were measured in several crystal samples with no applied field, and in KLTN as a function of applied field. The latter data are in agreement with a theory describing the coherent addition of a normal electrooptic grating and the Zefpr grating.

The authors acknowledge the support of the work by the Army Research Office, the Air Force Office of Scientific Research, and DARPA.

References

[1] R. S. Cudney et. al. , Opt. Lett. , 69, 67, (1992)

[2] P. M. Garcia, L. Cescato, J. Frejlich, J. Appl. Phys. 66 (1), 47, (1989)

[3] M. Z. Zha, P. Amrhein, and P. Günter, IEEE J. Q E, 26 (4), 788, (1990)

[4] W. B. Lawler, C. J. Sherman, and M. G. Moharam, J. Opt. Soc. Am. B, 8 (10), 2190, (1991)

[5] J. O. White, et. al. , *Photorefractive Materials and their Applications II*, chap. 4, eds. P. Günther and J. P. Huignard (Springer-Verlag, Berlin, 1989)

[6] R. Hofmeister and A. Yariv, App. Phys. Lett. , to appear Nov 16, 1992

[7] R. Hofmeister, et. al., Phys. Rev. Lett., 69 (9), 1459, (1992)

[8] A. Agranat, R. Hofmeister, and A. Yariv, Opt. Lett. , 69, 713, (1992)

Figure and Table Captions

Table 1. Values of the coupling constant g and the photorefractive phase ϕ for the crystal samples tested. The KLTN is paraelectric so its photorefractive response in the absence of an applied field is due to formation of zero phase Zepfr gratings. When a 2200V/cm field is applied (last row), the electrooptic gratings dominate, and the phase is far from zero.

Figure 1. The experimental setup for determining the photorefractive coupling constant and phase of dynamic gratings. The piezoelectric mirror PM modulates the phase of one beam either sinusoidally or as a ramp. The detector outputs are processed with a spectrum analyzer and x-y plotter.

Figure 2. The intensity $I_1(L)$ of figure 1 at ω and 2ω relative to the DC power (= 0 dB) when one of two interfering beams is phase modulated at ω, as a function of the photorefractive phase ϕ. The results are plotted for various coupling constants: gL = 3, 5, 10.

Figure 3. The photorefractive phase of gratings written in KLTN versus applied electric field. The data agree well with the theoretical curve describing the interaction between a Zepfr- and an electrooptic grating.

Figure 4. The coupling constant g of KLTN versus applied field. Again, the data are in accord with the theory as in figure 3.

Material	g /cm	ϕ - rad
$LiNbO_3$	13.3	0.41
$BaTiO_3$	2.30	1.47
KLTN	2.51	0.0
KLTN (2200V/cm)	6.88	1.05

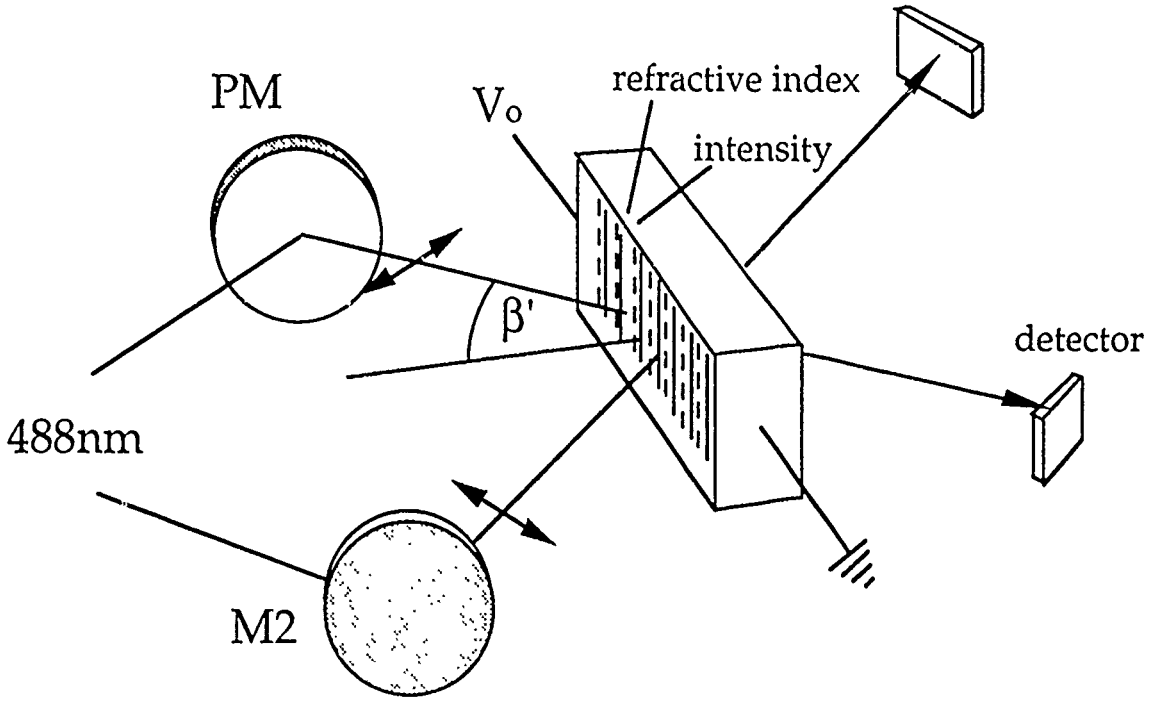
PM
Vo
refractive index
intensity
β'
detector
488nm
M2

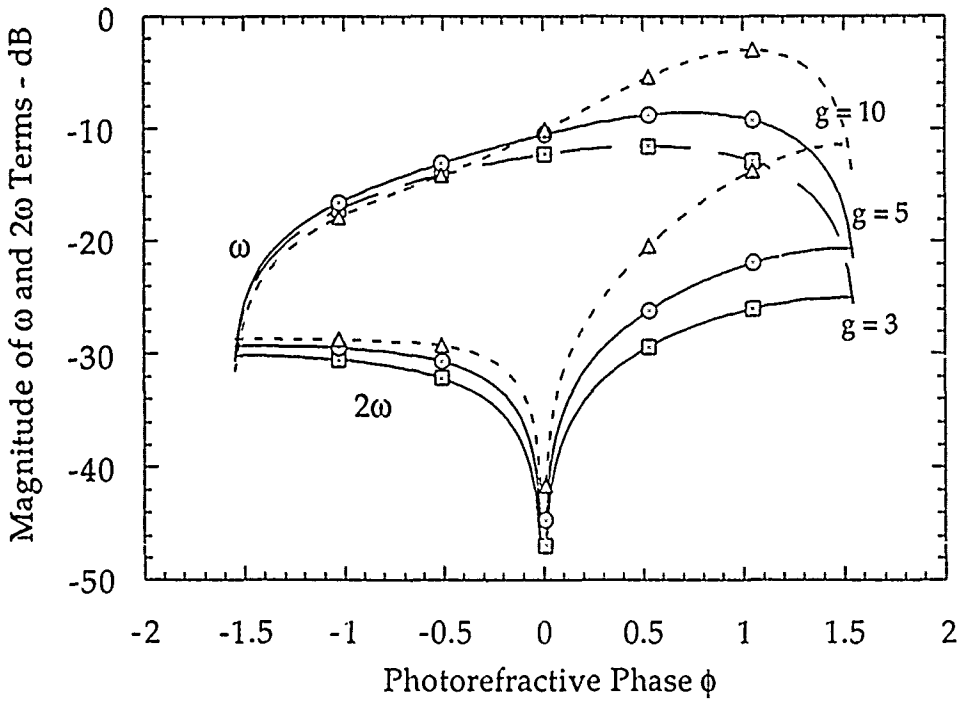
Magnitude of ω and 2ω Terms - dB
0
-10
-20
-30
-40
-50
-2
-1.5
-1
-0.5
0
0.5
1
1.5
2
Photorefractive Phase ϕ
ω
2ω
g = 10
g = 5
g = 3

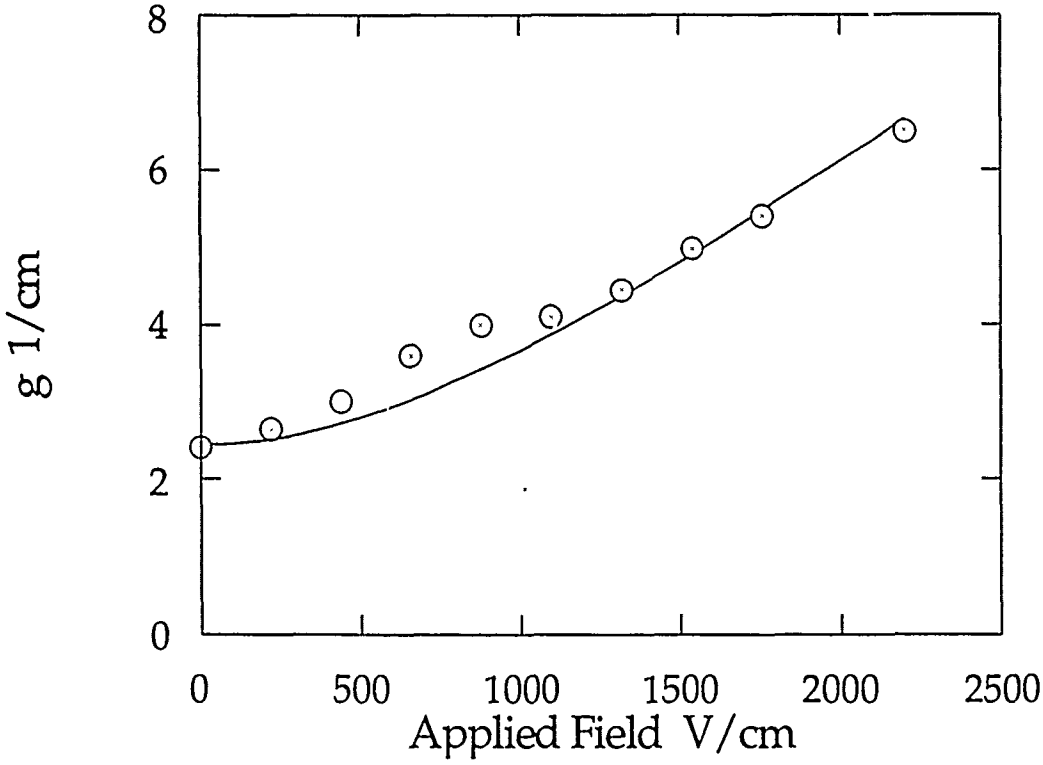
8
6
4
2
0
g 1/cm
0
500
1000
1500
2000
2500
Applied Field V/cm

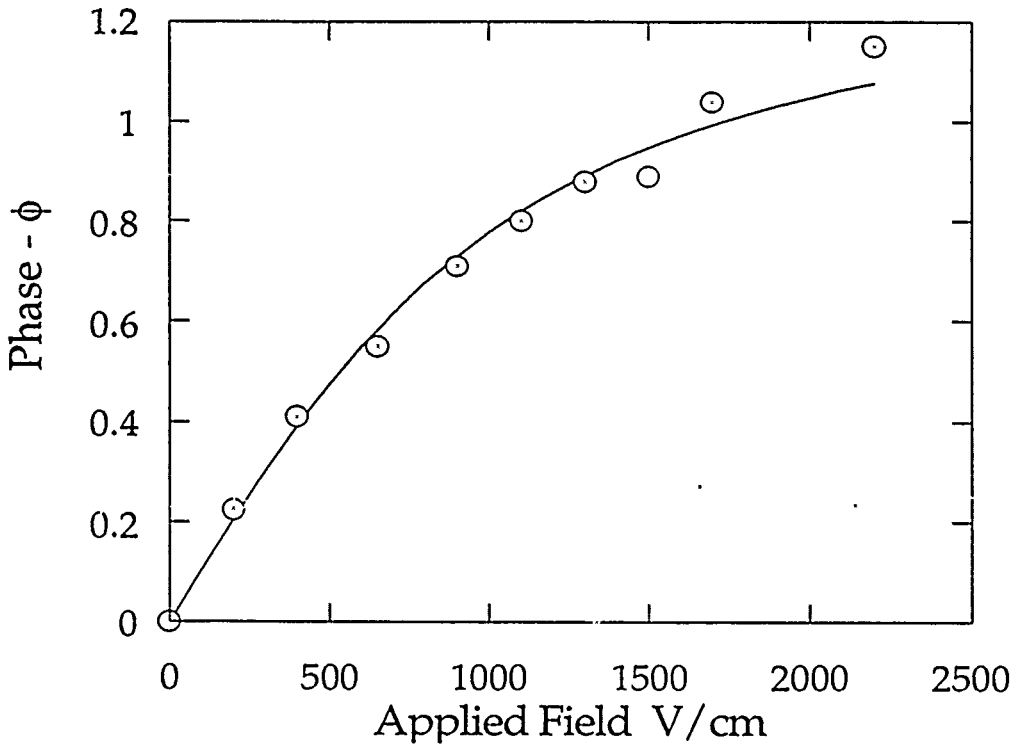
1.2
1
0.8
0.6
0.4
0.2
0
Phase - ϕ
0
500
1000
1500
2000
2500
Applied Field V/cm

a reprint from Optics Letters

APPENDIX D

Characterization of a new photorefractive material: $K_{1-y}L_yT_{1-x}N_x$

Aharon Agranat

The Hebrew University of Jerusalem, Jerusalem 91904, Israel

Rudy Hofmeister and Amnon Yariv

California Institute of Technology, Pasadena, California 91125

Received January 15, 1992

We report the growth and characterization of a new photorefractive material, potassium lithium tantalate niobate (KLTN). A KLTN crystal doped with copper is demonstrated to yield high diffraction efficiency of photorefractive gratings in the paraelectric phase. Voltage-controllable index gratings with $n_1 = 8.5 \times 10^{-5}$ were achieved, which yielded diffraction efficiencies of 75% in a 2.9-mm-thick sample. In addition, diffraction was observed in the paraelectric phase without an applied field. This effect is attributed to a growth-induced strain field.

The use of photorefractive materials to store volume holograms for optical computing and optical memories has long been an active area of research.[1-3] In addition, these materials show promise in the implementation of optical neural networks.

Potassium lithium tantalate niobate ($K_{1-y}L_yT_{1-x}N_x$) forms a solid solution for $y \leq 0.15$. Nevertheless, most research has been concentrated on the end members KLT[4,5] and KTN.[6,7] In general, most compositions of the solid-solution series have received little attention, possibly because they are considered difficult to grow.

We were able to grow large optical-quality crystals of KLTN using the top-seeded solution growth method by carefully choosing the constituent concentrations of the flux. Our primary motivation for adding lithium to KTN was to achieve a room-temperature phase transition[8] with a lower niobium concentration than that in conventional KTN's. Secondarily, the lithium ion is expected to be more mobile than the potassium ion that it replaces and is expected to weaken the transition from first order to order disorder.[9]

KLTN has the perovskite structure. In its highest symmetry phase it is cubic and, for small lithium concentrations, undergoes transitions to tetragonal, orthorhombic, and rhombohedral structures with decreasing temperature.[10] In our experiments the crystal was maintained just above the paraelectric/ferroelectric transition.

In the cubic phase the material's photorefractive properties are described by the quadratic electro-optic effect.[11] The birefringence is given by

$$\Delta n = \frac{n_0^3}{2} g P^2,$$

$$P = \epsilon_0(\epsilon - 1)E, \tag{1}$$

where g is the relevant quadratic electro-optic coefficient, n_0 is the index of refraction, and ϵ is the dielectric constant. P is the induced dc low-frequency polarization that we assume is linear with E. In this case, when an external field is applied to the crystal, an index grating is written with

$$n_1 \equiv \Delta n[E_0 + E_{sc}(x)] - \Delta n(E_0)$$

$$\cong \frac{n_0^3}{2} g\epsilon_0^2\epsilon^2[2E_0E_{sc}(x) + E_{sc}^2(x)]$$

$$\Rightarrow n_{1_{eff}} = n_0^3 g\epsilon_0^2\epsilon^2 E_0 E_{sc}(x), \tag{2}$$

where $E_{sc}(x)$ is the space-charge field due to the interfering light beams and E_0 is the applied field. $n_{1_{eff}}$ is the term of relation (2) that leads to Bragg matching. The space-charge field is thus transparent to the interfering beams unless a spatially uniform field is applied. By using this property, we have performed modulation of the nonlinear response at 20-kHz rates.

In this Letter we discuss the material properties of a KLTN crystal. We report a capacitive measurement of the dielectric constant that indicates that the KLTN undergoes a second-order phase transition. Diffraction experiments performed both with and without an applied field are described. Finally, KLTN is indicated to be a promising new photorefractive material.

The sample used in the following discussion was a 6.8 mm × 4.9 mm × 2.9 mm piece cut from a crystal grown by us using the top-seeded solution growth method. The crystal was pale olive green and free of striations. Its as-grown weight was 11.6 g. By using electron microprobe and atomic absorption analysis, the composition was determined to be $K_{0.950}Li_{0.04}Ta_{0.857}Nb_{0.129}:Cu_{0.004}$.

Figure 1 shows the absorption spectrum of the as-grown sample with peaks at 370 and 585 nm caused by Cu^{1+} donors and Cu^{2+} traps, respectively. The concentration of the impurities Cu^{1+} and Cu^{2+} can be determined from the absorption peaks by using

0146-9592/92/100713-03$5.00/0

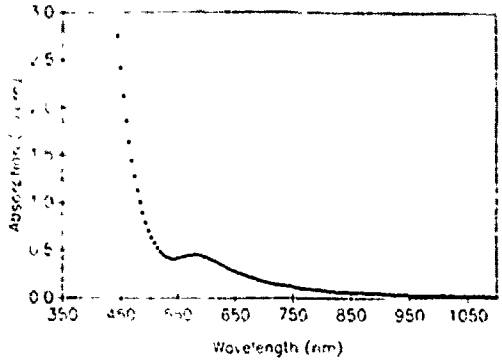

Fig. 1. Absorption spectrum of the as-grown KLTN:Cu.

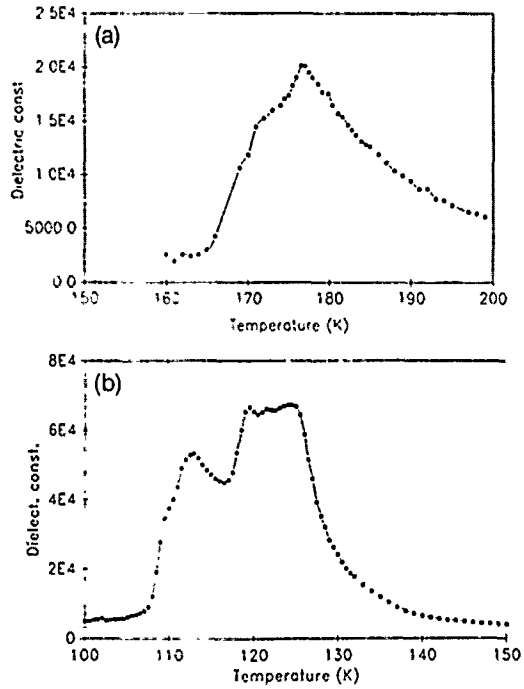

Fig. 2. (a) Dielectric constant of the $KLT_{0.857}N_{0.129}$. The phase transition is ~50 K higher than in a comparable KTN. (b) Dielectric constant of $KT_{0.86}N_{0.13}$.

Beer's law.[12] We calculate $[Cu^{1+}] = 6.0 \times 10^{19}/cm^3$ and $[Cu^{2+}] = 2.1 \times 10^{18}/cm^3$.

White-light birefringence measurements between crossed polarizers were used to measure the effective quadratic electro-optic coefficients. We determined $g_{11} - g_{12} = 0.186\ m^4\ C^{-2}$ to an accuracy of 5%.

The dielectric constant was monitored as a function of temperature by measuring the capacitance of the crystal, where $C = \epsilon_0 \epsilon A/d$. The results, shown in Fig. 2(a), are compared with those obtained from a KTN crystal with a similar tantalum:niobium ratio [Fig. 2(b)]. The cubic/tetragonal transition temperature has been raised approximately 60 K, to 178 K. The FWHM, i.e., the temperature range over which the dielectric constant drops to half its maximum value, is increased to ~10 K. Diffraction due to the linear electro-optic effect was weak directly below the transition and grew steadily as the temperature was lowered, indicating a second-order transition.

The diffraction experiments with applied field were performed as in Fig. 3 with the sample maintained at a temperature of 15 K above the transition. The writing argon laser beams were at either 488 or 514 nm. They were ordinary polarized to minimize beam interaction. The diffraction efficiency of the grating thus written was monitored with a weak extraordinary-polarized He–Ne beam at 633 nm. The 633-nm beam was verified not to erase the grating. The writing continued until the maximum diffraction was achieved.

After the gratings were written, the crystal was cooled to just above the transition, and the diffraction efficiency was determined as a function of applied field. The results are illustrated in Fig. 4. The three curves shown are for gratings that were written at +1450, 0, and −1450 V/cm. When the grating was optically erased with the argon beams, some residual diffraction (~1%) remained that was not optically erasable and could only be removed by heating the crystal to room temperature.

The highest diffraction efficiency observed for 488-nm writing beams was 75% for a sample of thickness 2.9 mm, where corrections were made for Fresnel losses. For 514-nm writing beams, the maximum value was reduced to 30%, and at 633 nm the diffraction was almost undetectable. The writ-

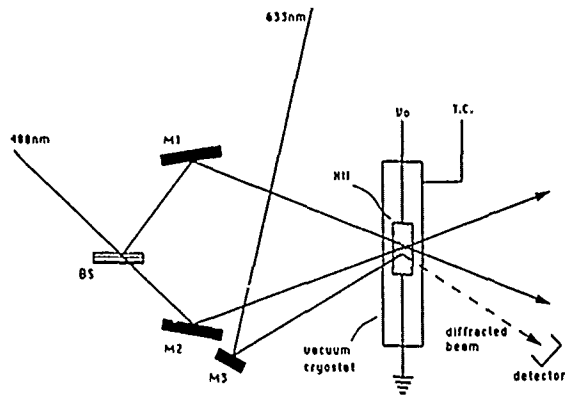

Fig. 3. Experimental setup for measurement of diffraction efficiency. Photorefractive crystal Xtl is mounted in a vacuum cryostat. Beam splitter BS and mirrors M1 and M2 create a 488-nm grating that is read with the Bragg-matched 633-nm beam and mirror M3. Diffraction is measured versus applied voltage Vo. The temperature was monitored by thermocouple T.C.

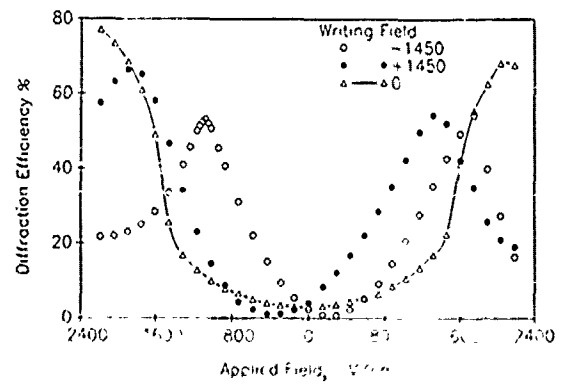

Fig. 4. Two-beam diffraction efficiency for gratings written at +1450, 0, and −1450 V/cm.

ing times for maximum diffraction roughly followed $\tau_{write} \approx 6\ s^2 cm^2 W^{-1}$ light intensity incident upon the crystal.

From the calculated index modulation of $n_1 = 8.5 \times 10^{-5}$, we determine the space-charge field to be $E_{sc} = 150$ V/cm. Using the writing time of 180 s at beam intensities adding up to 27.2 mW, we estimate the sensitivity for this KLTN crystal to be 7.30×10^{-6} cm^3/J for an applied field of 1.6 kV/cm. Following the procedure outlined above, the erase time near T_c was up to 2 orders of magnitude greater than the write time at $T_c + 15$ K.

KLTN was also observed to display weak diffraction without an applied field at as much as 120 K above the phase transition. At room temperature the diffraction efficiency in a 3-mm-thick sample was 0.65%. The effect was strongest with focused beams and weakened as progressively larger areas of the sample were illuminated. However, the diffraction efficiency measured with a given beam geometry was independent of beam intensity over several orders of magnitude.

In the diffraction experiments performed, an index grating was generated as in relation (2). Thus the diffraction efficiency in the crystal is a strong function of the dielectric constant ϵ. The largest effects occur near the phase transition. In KLTN the lithium raised the transition temperature 60 K over that of a KTN cyrstal with similar niobium concentration so that the temperature of maximum response was correspondingly raised. By choosing the proper niobium and lithium concentration, it may be possible to raise T_c to near room temperature while retaining a second-order transition.

As reported, the diffraction due to the linear electro-optic effect was weak directly below the transition and grew steadily as the temperature was lowered. The fact that the linear electro-optic coefficients are known to be large in this class of materials indicates that there is little spontaneous polarization at the transition. In other words, the transition displays second-order behavior and is at best weakly displasive. This agrees with KTN studies in which the phase transition is reported to become first order only for niobium concentrations exceeding 30%.[10]

In the experiments of diffraction with an applied field, the data are seen to follow a $\sin^2$ behavior with saturation (Fig. 4). This saturation is at least partly due to nonlinear polarizability of the medium at high field strengths.[6] From the data it is clear that a compensating dc field of approximately 300 V/cm is induced in the crystal under the influence of the writing field. As described previously, residual diffraction persisted when the gratings were optically erased. Also the erase/write time asymmetry was increased by up to 2 orders of magnitude. The asymmetry in the erasure time close to the transition may be due to the following mechanism: It is well known that in these crystals dipolar clusters are formed around impurities that move outside the center of inversion. In the vicinity of the phase transition the correlation length of these clusters becomes large and their relaxation time increases. Thus it is possible that a secondary grating is formed by these dipolar clusters in addition to the normal space-charge grating. The erasure time of the secondary grating is long in the vicinity of the phase transition, and this causes the asymmetry. This tentative explanation is currently under further investigation. We hope to harness this effect in the future to perform fixing in these materials.

In the experiments without an applied field, it was observed that substantial diffraction only occurs when the writing beams interfere over a small (uniformly strained) region of the crystal. We have determined that the effect arises from a weak semi-uniform strain that is due to the growth proces

In conclusion, we have demonstrated the growth of a new photorefractive material, KLTN, and have characterized its photorefractive properties. Strong quadratic electro-optic coefficients, high diffraction efficiences, and sensitivities of 7.30×10^{-6} cm^3/J at 1.6 kV/cm were observed. Based on this research, KLTN crystals seem to be highly promising materials for volume hologram storage applications. In addition, the aspect of voltage control leads naturally to various interconnect schemes for neural networks.

This research is supported by the U.S. Army Research Office.

References

1. P. J. Van Heerden, Appl. Opt. **2**, 393 (1963).
2. D. Gabor, IBM J. Res. Dev. **13**, 156 (1969).
3. D. Von der Linde and A. M. Glass, Appl. Phys. **8**, 85 (1975).
4. Y. Yacoby and A. Linz, Phys. Rev. B **9**, 2723 (1974).
5. J. J. Van der Klink and D. Rytz, J. Cryst. Growth **56**, 673 (1982).
6. A. Agranat, V. Leyva, and A. Yariv, Opt. Lett. **14**, 1017 (1989).
7. R. Orlowski, L. A. Boatner, and E. Kraetzig, Opt. Commun. **35**, 45 (1980).
8. K. Sayano, Accuwave, Santa Monica, Calif. 90404 (personal communication, 1990).
9. R. L. Prater, L. L. Chase, and L. A. Boatner, Phys. Rev. B **23**, 5904 (1981).
10. C. M. Perry, R. R. Hayes, and N. E. Tornberg, in *Proceedings of the International Conference on Light Scattering in Solids*, M. Balkansky, ed. (Wiley, New York, 1975), p. 812.
11. A. Agranat, K. Sayano, and A. Yariv, in *Digest of Meeting on Photorefractive Materials, Effects, and Devices* (Optical Society of America, Washington, D.C., 1987), paper PD-1.
12. V. Leyva, Ph.D. dissertation (California Institute of Technology, Pasadena, Calif., 1991).

New Photorefractive Mechanism in Centrosymmetric Crystals: A Strain-Coordinated Jahn-Teller Relaxation

Rudolf Hofmeister, Amnon Yariv, and Shogo Yagi[a]
California Institute of Technology, Pasadena, California 91125

Aharon Agranat
Hebrew University of Jerusalem, Jerusalem, Israel
(Received 19 March 1992)

We present observations and an explanation of a photorefractive effect in strained centrosymmetric KTN and KLTN crystals in the absence of an externally applied electric field. Centrosymmetric crystals are forbidden to display the classical photorefractive effect without application of an applied field. Nevertheless, in diffraction experiments, centrosymmetric KTN:Cu and KLTN:Cu crystals show index changes of up to 1.7×10^{-5} and photorefractive response at more than 120 °C above the phase transition. Experiments described here allow us to conclude that a Jahn-Teller relaxation of the spatially modulated Cu^{2+} dopant concentration is responsible.

PACS numbers: 78.20.Hp, 42.70.−a, 42.65.−k

The photorefractive properties of potassium tantalate niobate (KTN) were identified more than fifteen years ago [1] but the difficulty of growing high-quality crystals hindered their study until recently. When the crystals are illuminated by a spatially periodic intensity pattern the resulting charge redistribution results in a spatially periodic electric field $E_{sc}(x)$ which leads, via the electro-optic effect, to an index grating $\delta n(x)$. We have succeeded in growing optical quality KTNs and potassium lithium tantalate niobates (KLTNs) with high dopant concentrations and wide ranges of lithium and niobium concentrations [2]. Recent investigations of these crystals have revealed a photorefractive response which cannot be explained by the conventional electro-optic theory. This new effect is expected to occur in most transition metal doped perovskites especially when a strain is present. In the KTNs and KLTNs reported on here, the strain is due to the growth process.

Perovskite oxide photorefractives operated above the phase-transition temperature (paraelectric and centrosymmetric phase) lack a linear electro-optic coefficient. Instead, the photorefractive mechanism in these symmetric materials arises through the quadratic electro-optic effect. Here the Bragg matched term of the index grating due to a spatially periodic field $E_{sc}(x)$ in the presence of an applied electric field E_0 can be written [3] as $\delta n = n_0^3 g(\varepsilon\varepsilon_0)^2 E_0 E_{sc}(x)$, where g is the relevant quadratic electro-optic coefficient, and n_0 the index of refraction. We assume that the polarization is linear ($P=\varepsilon E$) and that the dielectric constant $\varepsilon \gg 1$. Thus the conventional photorefractive effect is zero in the absence of a spatially uniform electric field.

Nevertheless, our experiments reveal the existence of a zero electric field photorefractive (ZEFPR) effect in KTN and KLTN at temperatures at least 120 °C above the phase transition where the crystal is nominally symmetric. No effect is seen with undoped crystals or with thermally reduced samples. The diffraction expected from absorption gratings is 3 orders of magnitude too weak to explain the effect. The studies of the phenomena which are described here reveal a new photorefractive mechanism. In this paper we describe the effect and present what we believe is the most plausible explanation. The experimental results supporting the explanation follow and, finally, we give results of a theory of Jahn-Teller relaxation.

The zero external field photorefractive (ZEFPR) effect was first noticed by us [3,4] in KTN and KLTN crystals. This photorefractive effect was attributed to the presence of a growth induced strain [5]. In addition, Yang *et al* [6] have cited an "extremely small" effect in KTN in the absence of an applied field, but without explanation. Recently, we have developed a method of producing KTNs and KLTNs with high niobium concentrations of high optical quality, and in these crystals, the effect is greatly enhanced. Under certain conditions of crystal preparation we have been able to produce zero field index gratings with $\Delta n = 1.7\times10^{-5}$, and diffraction efficiencies of over 20% in a 4.15-mm-thick sample using 488-nm argon laser beams.

In the crystals which displayed a strong ZEFPR effect, the photorefractive dopant was copper, which is stable as either Cu^{1+} or Cu^{2+}. The Cu^{2+} ion is known to cause large Jahn-Teller (J-T) distortions, especially in octahedral symmetry. The Cu^{1+} ion by contrast, has no tendency to distort. The illumination of the crystal by the periodic intensity pattern of the optical field leads to a mimicking spatially periodic Cu^{2+}/Cu^{1+} ratio due to excitation of electrons (from Cu^{1+}) and trapping by Cu^{2+}. This, as explained above, gives rise to a spatially periodic distortion [7]. Since the copper concentration is relatively small in the KLTNs we do not expect a cooperative ordering of the distortions, rather, their orientation should be random. But when a macroscopic (growth induced)

strain is present, as is the case in the crystals studied, the distortions will orient preferentially in order to minimize that strain. The result is a spatial modulation of the strain field in phase with the intensity which leads to a corresponding modulation of the index of refraction (index grating) via the photoelastic effect. We expect this phenomenon to be quite general, although only noticeable when the conventional photorefractive effect is forbidden.

The strain in the crystals is due to the particulars of the growth process; we describe it only briefly here since it is discussed in detail elsewhere [2]. The crystal grows as a series of cubical shells, expanding from the seed. During the growth the composition of the crystal changes which is attendant by an increase in the lattice constant. Thus each face of the cubical shell of the growing crystal must be compressed slightly to mesh with the previous cubical shell. In this way there arises a compressive strain in the plane of each face of the cube which increases with distance from the seed crystal. Similarly, there is also a tensile strain perpendicular to each face of the cube which also increases with distance from the seed. These strains induce a linear birefringence which is readily apparent when the crystal is viewed through crossed polarizers. When a small sample is cut from the grown crystal near the center of one of the cube faces, the strain in the sample will be homogeneous: uniformly compressive in two directions and uniformly tensile in the third.

To test the validity of the theory of J-T relaxation we investigated the dependence of the index grating on the strain present in the crystal. The experimental setup for performing diffraction experiments is illustrated in the inset of Fig. 3. Two extraordinary beams at 488 nm symmetrically incident, created an optical intensity standing wave inside the sample. After several minutes, one of the beams was blocked with an electronic shutter for 50 msec. While the shutter was closed we measured the optical power which was diffracted by the grating into the direction of the blocked beam. The diffraction efficiency, η, is defined as the ratio of the diffracted power to the power incident on the crystal. We corrected for losses from facet reflections.

Unless otherwise indicated, all measurements were performed at room temperature on several KTNs and KLTNs. We determined that in homogeneously strained samples the diffraction efficiency increased as the square of the interaction length and was independent of total intensity. We constructed a two-dimensional vise to be able to compensate the growth induced strain with external pressure applied in two dimensions The diffraction efficiency in a 2.85-mm-thick sample was reduced by 40% when the internal strain was minimized Additionally, the effect is reduced when the sample is exposed to heat treatments which reduce the internal strain but which leave the conventional photorefractive properties unchanged [8].

Although this evidence shows that the ZEFPR effect relies partially on the macroscopic strain, it remains to be shown that the strain does not induce a morphic lowering of the crystal symmetry, allowing a linear electro-optic coefficient. We tested for the existence of a linear electro-optic effect in a sample of $K_{0.994}L_{0.0006}T_{0.700}N_{0.299}$ by measuring the birefringence induced under application of electric fields in various directions. A Soleil-Babinet compensator between crossed polarizers oriented at 45° to the crystal axes was used to measure the birefringence at 633 nm. The results were fitted to a third-order polynomial but the best fit was purely quadratic to the resolution of the experiment. Measurements were repeatable to $\delta(\Delta n) < 5\times10^{-7}$. This indicates an almost perfect quadratic electro-optic effect with $g_{11}-g_{12}=0.123$ m^4C^{-2}, which agrees with previously published values for KTN [9]. It should be noted that the absence of a third-order term indicates little or no polarization nonlinearity. We conclude that the strain does not induce a linear electro-optic coefficient.

Next, a series of experiments were performed to verify anticipated characteristics of the ZEFPR effect. For these experiments a $K_{0.990}L_{0.0019}T_{0.730}N_{0.27}$:Cu sample was used, where $[Cu^{2+}]=3.1\times10^{18}$ cm^{-3}, determined from optical absorption data [10]. The crystal was centrosymmetric above its phase transition at $T_c\sim-23$ °C.

First, since the ZEFPR effect is due to a strain "grating" which modulates the refractive index via the photoelastic effect, we expect at most weak dependence on the dc/low-frequency dielectric constant ε. We confirmed this by measuring the dependence of the ZEFPR effect on temperature near the phase transition (here ε obeys the Curie-Weiss law). Using the setup as in Fig. 3, two interfering 488-nm beams with equal intensities of ~500 $mW cm^{-2}$ uniformly illuminated the crystal. No field was applied during writing of the diffraction grating. After a writing time of 60 s, one beam was blocked and the other beam attenuated to minimize erasure, and the resultant diffraction was measured. After the diffraction due to the ZEFPR effect was determined, a field was applied to determine the index change due to the quadratic electro-optic effect. Finally, after each measurement, the gratings were completely erased by flooding the crystal with uniform illumination and raising the temperature, if necessary. The results for various temperatures are illustrated in Fig. 1. The quadratic effect increases dramatically as the phase-transition temperature (-23 °C) is approached because of the concomitant increase in dielectric constant. The extremely high diffraction efficiencies with a $\sin^2$ rollover at high fields are characteristic of the quadratic effect in centrosymmetric KLTN [3,4]. The $\sim1\%$ diffraction efficiency observed at zero electric field is caused by the ZEFPR effect. It is independent of the dielectric constant since it is nearly a constant for the seven temperatures investigated which range through the ferroelectric transition at -23 °C. Although the ZEFPR effect diffraction is weak in the configuration used for this

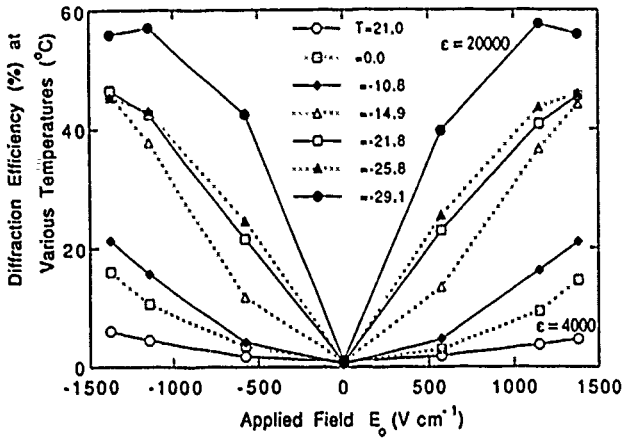

FIG. 1. The diffraction efficiency vs applied field and temperature for an index grating written with zero applied field. The small zero-field value is independent of temperature, whereas the quadratic electro-optic contribution increases by more than an order of magnitude.

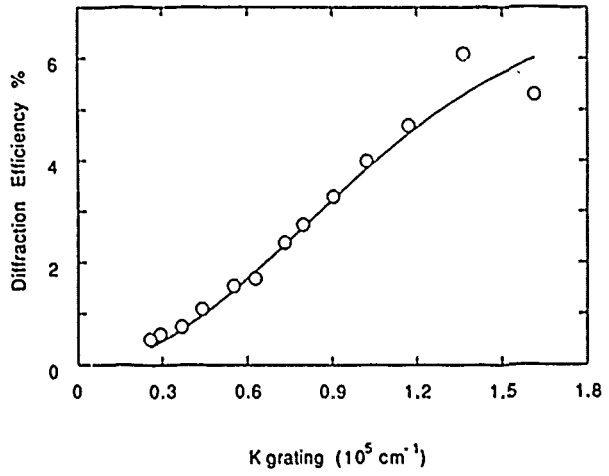

FIG. 2. Diffraction efficiency vs the grating K vector for a 4.15-mm KLTN crystal. The curve shows the best fit to Eq. (1) with $N_a = 2.8\times10^{18}$ cm^{-3}, in agreement with results from optical absorption data.

experiment, the same sample yielded over 20% diffraction efficiency at a higher angle of beam incidence. The fact that the ZEFPR index grating has no noticeable dependence on the dielectric constant proves that the effect is distinct from the quadratic electro-optic effect. The ZEFPR effect is a new phenomenon which has nothing to do with the polarization caused by a space charge field ($P=\varepsilon E$).

Our model stipulates that the magnitude of the ZEFPR index grating depends linearly on the spatial modulation of the Cu^{2+} ions. Since the Cu^{2+} modulation is equal to the modulation of the photoexcitable charge carriers, we expect the ZEFPR index grating to have the same functional dependence as the light-induced space-charge electric field caused by the charge modulation. From the basic Kukhtarev model for the space charge field induced by the interfering beams we have [11]

$$E_{sc} = i\frac{(2I_1I_2)^{1/2}}{I_1+I_2}\frac{KTk/e}{1+K^2kT\varepsilon/e^2N_A}\cdot\cos2\theta, \qquad (1)$$

where θ is the angle of beam incidence in the crystal, I_1 and I_2 are the beam intensities, and K is the index grating wave vector. The dependence on E_{sc} was tested by monitoring the diffraction efficiency as a function of the grating wave vector and the beam intensity ratios. We determined a relation between the index change and the space charge field for the ZEFPR effect from the $E_0=0$ data of Fig. 1 to be $\Delta n_{ZEFPR} = 5\times10^{-9}E_{sc}$ in cgs units. Figure 2 shows the diffraction efficiency versus K. Peak diffraction efficiency of 6.1% was observed, corresponding to $\Delta n = 9.1\times10^{-6}$. The best fit of the data to Eq. (1) occurs for $N_a = 2.8\times10^{18}$ cm^{-3}, which is near the value (3.1×10^{18} cm^{-3}) obtained from absorption data. Figure 3 plots the diffraction versus beam intensity ratios, along with the theoretical curve from Eq. (1). The good correspondence of the data in Figs. 2 and 3 with Eq. (1) allows us to conclude that the index change of the ZEFPR effect varies as the space charge field.

Our final test of the ZEFPR effect was to measure the phase of the ZEFPR index grating relative to the intensity grating of the writing beams. Since the index grating is modulated by the local Cu^{2+} concentration, we expect it to be in phase with the intensity, so that no two-beam coupling (power exchange between the two writing beams) will occur. This condition was verified by testing for two beam coupling with the setup of Fig. 3. No power transfer was observed even though strong diffraction occurred when either beam was blocked. Two-

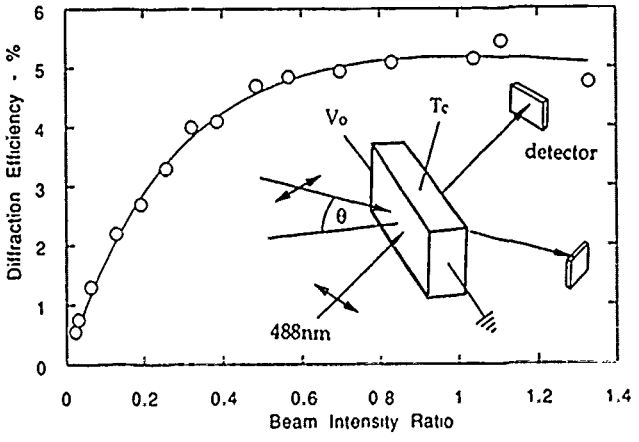

FIG. 3. The diffraction efficiency of a KLTN crystal vs the beam intensity ratios. The curve is the theoretical dependence of the space charge field on the modulation depth. Inset. The experimental geometry. V_0 is the applied voltage (=0 when measuring the ZEFPR effect), and Tc is the temperature control.

beam coupling was observed, however, when an electric field was applied. The zero phase of the ZEFPR gratings further confirms the distinction of the ZEFPR effect from electro-optic mediated photorefractive effects where the phase must be nonzero because it is due to the intrinsically nonlocal space charge field.

The tests described above form the basis for our conclusion that the ZEFPR effect is caused by a Jahn-Teller relaxation in conjunction with the photoelastic effect. In what follows we present a simple theory of the interaction between the local J-T distortions and a macroscopic strain field. We consider a crystal with a growth induced tensile strain along the x axis ($u_1 > 0$). The energy of the strained crystal per unit volume is given by $E = (u_1^2/2)[c_{11} - 2c_{12}\sigma]$, where the usual index contraction is used, σ is Poisson's ratio, and c_{ij} are the elastic constants.

The J-T distorting centers distributed randomly throughout the volume of the crystal will alter the strain so that $u_i' = u_i + \Delta u_i$ where Δu_i is the change in macroscopic strain due to the summation of the individual J-T distortions. The individual distortions are elongations of the oxygen octahedra in one of three orthogonal directions. We denote y as the fraction of distorting centers oriented along the x axis, and $(1-y)$ as the remaining fraction distributed along either the y or the z axes. We readily determine $\Delta u_1[y] = \Delta u_1[1][(1+\sigma)y - \sigma]$, where $\Delta u_1[1]$ is the strain change when $y = 1$ (complete ordering).

The decrease in elastic energy per unit volume resulting from the reduction in strain $\Delta u_i[y]$ is obtained as $\Delta E[y] = -u_1 \Delta u_1[y][c_{11} - 2c_{12}\sigma]$. The entropy change of the ordering follows readily by counting the number of configurations of the distortions. There are (ny) distorting centers oriented along the x axis per unit volume, and $n(1-y)$ oriented along either the y or z axes. The entropy change $(\Delta S = k \ln W)$ is found to be $\Delta S[y] = -nk\{y \ln[y] + (1-y)\ln[(1-y)/2]\}$. Minimizing the free energy yields the temperature dependence of the ordering parameter. We calculate that

$$y[\beta] = e^{\beta U}/(e^{\beta U} + 2), \tag{2}$$

where the "strain alignment energy" per distorting center $U = \Delta E[1](1+\sigma)/n$ and $\beta = 1/kT$. From this we conclude that large macroscopic strains lead to ordering of distortions; our preliminary results indicate that $\beta U \sim -0.4$ so that the partial ordering occurs.

Finally, the index grating results from the periodic change in the optical impermeability tensor, $\delta\beta_{ij} = p_{ij}\delta(\Delta u_j[y])$, where $\delta(\Delta u_j[y])$ is the periodic strain variation calculated above and p_{ij} are the photoelastic constants. We note that even in the absence of macroscopic strain $\delta\beta_{ij} \neq 0$ unless $\sigma = 0.5$. The determination of the parameters of this theory, particularly $\Delta u_i[y]$, is ongoing

R.H. would like to acknowledge the many valuable discussions with Dr. Mordechai Segev. This research was performed under a U.S. Army Research Office grant.

---

[a]Permanent address: NTT Interdisciplinary Research Laboratories, Ibaraki, Japan.

[1] F. S. Chen, J. Appl. Phys. **38**, 3418 (1967).

[2] R. Hofmeister, A. Agranat, and A. Yariv (to be published).

[3] A. Agranat, V. Leyva, and A. Yariv, Opt. Lett. **14**, 1017 (1989).

[4] A. Agranat, R. Hofmeister, and A. Yariv, *Technical Digest on Photorefractive Materials, Effects, and Devices* (Optical Society of America, Washington, DC, 1991), Vol. 14, p. 6.

[5] R. Hofmeister, A. Agranat, and A. Yariv, Opt. Lett. **17**, 713 (1992).

[6] Changxi Yang *et al.*, Opt. Lett. **17**, 106 (1992).

[7] In the work of H. Liu, R. C. Powell, and L. A. Boatner, Phys. Rev. B **44**, 2461 (1991), transient gratings from lattice relaxation in KTN are reported. But the mechanism described is electronic excitation caused by two-photon absorption. The mechanism described here is new because it arises from transport and static Jahn-Teller distortion.

[8] V. Leyva (private communication).

[9] F. S. Chen *et al.*, J. Appl. Phys. **37**, 388 (1966).

[10] V. Leyva, Ph.D. thesis, California Institute of Technology, 1991 (unpublished).

[11] N. V. Kukhtarev *et al.*, Ferroelectrics **22**, 949 (1979).

Best Available Copy

APPENDIX F

Docket No. 90-204

METHOD AND APPARATUS FOR ALL-OPTICAL HOLOGRAPHIC PHASE MODULATION AND MOTION SENSING

BACKGROUND OF THE INVENTION

This invention was made with government support under U.S. Army Contract No. DAAL-03-91-G-0305. The U.S. government has certain rights in the invention.

1. Field Of The Invention

The present invention relates to phase modulation and motion sensing devices and more particularly to a method and apparatus for performing all-optical, self-aligning, holographic phase modulation and motion sensing utilizing a zero external electric field photorefractive effect in paraelectric materials.

2. Description Of The Prior Art

Modernly, a wide variety of sensing devices, including electrical, mechanical and optical sensors, as well as various combinations of such sensors, are utilized in a large number of applications, including manufacturing and testing, research and development, information processing, communications, consumer products, and military applications, to name just a few. Various advantages and disadvantages, relating to a host of factors, including size, sensitivity, stability, responsiveness, alignment difficulty and cost, to name just a few, are attendant upon different types of sensors and are of critical concern depending upon the particular application or need to which a sensor is to be addressed. To this end, sensor technology is a rapidly growing field with great attention being paid to new and innovative types of sensors and sensing methods. In particular, all-optical sensors and sensing methods are presently receiving considerable attention for use in applications where electrical signals cannot be used or are impractical. Such applications include, but are not limited to, aqueous, explosive, corrosive and electromagnetically sensitive environments.

With respect to all-optical sensors, intensity modulating sensors, primarily because of their relative ease of alignment, have traditionally been preferred over interferometric or phase modulation techniques. However, even intensity modulating all-optical sensors have significant alignment problems, typically due to the precise component positioning required to obtain good sensor sensitivity. These alignment problems also result in sensors that are not mechanically robust.

Thus, a need exists for an all-optical sensor and sensing method that may be used in applications where electrical signals are forbidden or are impractical, that is relatively mechanically robust, that provides ease of alignment and that operates via a phase modulation, rather than an intensity modulation, technique.

SUMMARY OF THE INVENTION

Accordingly, a principal object of the present invention is to provide an all-optical sensor and sensing method suitable for use in applications and environments where electrical signals cannot be used or are impractical.

A further object of the present invention is to provide an all-optical sensor and sensing method that are self-aligning.

Yet another object of the present invention is to provide an all-optical sensor and sensing method that utilizes phase modulation, as opposed to intensity modulation, techniques.

Yet a further object of the present invention is to provide an all-optical sensor and sensing method that are more mechanically robust than prior all-optical sensors.

In accomplishing these and other objects, there is provided an all-optical sensor comprising a crystal exhibiting a zero electric field photorefractive effect, which effect is described more fully hereinbelow, a phase modulation or vibration source or mechanism, a source of coherent optical radiation, a beam splitter mechanism and one or more optical radiation detectors. The output beam from the optical radiation source is split into first and second beams by the beam splitter and

one or both beams is phase modulated. The beams are directed through the photorefractive crystal exhibiting a zero electric field photorefractive effect, and the resultant transmitted beams are detected by one or more optical radiation detectors to provide a measurement of the phase modulation of the beams.

The all-optical sensor of the present invention is able to function in the absence of an electric field because of the zero electric field photorefractive effect (Zefpr effect) of its crystal, which effect has unique characteristics.

Generally, photorefractive effects are manifested as a change in the refractive index of a material when the material is exposed to light. When such a material is illuminated with two or more coherent laser beams, the intensity grating formed through the interference of the laser beams creates a holographic index of refraction grating, or index grating, spatially correlated with the intensity grating. This index grating can cause beam coupling, i.e., power transfer between the beams, with the degree of coupling being determined by the relative phase between the intensity and index gratings. In conventional photorefractive materials, the relative phase between the two gratings is, in general, non-zero. This is a fundamental consequence of the fact that the conventional photorefractive effect arises through the space charge field, which is a non-local effect.

In contrast, the Zefpr effect is due to a local strain relaxation in the crystal created by various photorefractive transition metal dopants in the crystal. The Zefpr effect has been observed in paraelectric KTN (potassium tantalate niobate) and KLTN (potassium lithium tantalate niobate) crystals whose photorefractive dopant was copper. Other candidates expected to exhibit the Zefpr effect include strontium barium niobate, potassium titanyl phosphate, barium titanate, strontium barium titanate and lithium niobate. In a Zefpr effect material, the holographic index grating is modulated by the local concentration of photorefractive transition metal dopants. Consequently, the index grating is in phase spatially with the intensity grating and no beam coupling will occur. This gives rise to the unique circumstance whereby

if either the phase of the index grating or of the interfering beams is modulated with a phase change very much less than π/2, the intensity of the beam transmitted through the Zefpr crystal will vary linearly with the modulation. This linear modulation allows crystals exhibiting the Zefpr effect to remotely sense phase modulations of any type in the absence of any electrical signals in the vicinity of the sensor.

A further aspect of Zefpr crystals is that their detection element consists of a holographic index grating that is continually being rewritten by the intensity grating resulting from the interfering laser beams in the crystal. This results in a sensing device that is self-aligning and resistant to mechanical shocks, thereby exhibiting a more robust mechanical nature than other all-optical sensors.

Further, due to the present invention's ability to operate in an environment where an electric field is prohibited or not practical, it has an enormous number of potential applications. For example, it may be used in corrosive or explosive environments. It may also be used in underwater applications as, for example, an optical hydrophone or underwater detection mechanism. It may also be used to create an untappable optical communications link of great stability. In addition, because the present invention's all-optical sensor is suitable for sensing any type of phase modulation, and is not simply limited to mechanical vibrations, it can be used as a high-speed phase-to-intensity data link that would be actuated through modulation of one of the two input beams by an electro-optic modulator. Such a data link would have a distinct advantage over conventional Mach-Zender type data links in that it is self-aligning, thus compensating for undesired path length changes. The result would be a data link that does not require active path length matching and which is also mechanically robust.

Other objects, characteristics and advantages of the present invention will become apparent from a consideration of the following detailed description with reference to the accompanying drawings.

BRIEF DESCRIPTION OF THE DRAWINGS

FIG. 1 is a schematic representation of one preferred embodiment of the present invention showing an acoustic phase modulation source and a Zefpr crystal functioning as a beam splitter.

FIG. 2 is a schematic representation of a preferred embodiment of the present invention showing an acoustic phase modulation source and a separate prism acting as a beam splitter.

FIG. 3 is a schematic representation of a preferred embodiment of the present invention with a piezo-electric mirror acting as a phase modulation source and a prism acting as a beam splitter.

FIG. 4 is a schematic representation of a preferred embodiment of the present invention showing phase modulation detection through interference of counterpropagated phase transparencies imaged onto a Zefpr crystal.

DETAILED DESCRIPTION OF THE INVENTION

Referring now to the drawings, wherein like numerals represent like parts throughout the several figures, FIG. 1 shows one preferred embodiment of the all-optical, self-aligning, holographic phase modulation sensing device 10 of the present invention. Sensing device 10 includes Zefpr crystal 12, phase modulation or vibration source 14, coherent optical radiation source 16 and optical radiation detectors 18. Zefpr crystal 12 exhibits the zero electric field photorefractive effect, described more fully hereinabove, that forms the basis of the present invention. Zefpr crystal 12 is, in this embodiment of the present invention, formed into a prism-like shape. In this fashion, Zefpr crystal 12 acts as the beam splitting mechanism of the beam of coherent optical radiation produced by optical radiation source 16. The two beams within Zefpr crystal 12 create an intensity grating which in turn forms an index of refraction grating that is continually being rewritten within Zefpr crystal 12. The grating rewrite time is a function of the incoming optical

radiation and is given by $\tau \approx 0.1 sec/I$ where I is the intensity incident in watts/cm^2. If the phase modulation introduced into Zefpr crystal 12 has a much higher frequency than the inverse of the grating rewrite time, then the grating will not be erased.

Acoustic phase modulation source 14 produces a phase modulating output which, as represented by line A, is coupled into Zefpr crystal 12 where it modulates the phase difference between the intensity grating and the index grating in Zefpr crystal 12. As a result of the zero electric field photorefractive effect exhibited by Zefpr crystal 12, the modulation of the phase between the index grating and the intensity grating results in a linear variation of the transmitted intensity of the split beams in crystal 12. This linear variation is then detected by detectors 18 and analyzed to provide a measurement of the phase modulation output of phase modulation source 14. Because of the nature of the zero electric field photorefractive effect exhibited by crystal 12, this measurement may be accomplished in an environment where an electrical signal cannot be used or is impractical.

Turning now to FIG. 2, there is shown another preferred embodiment of the all-optical, self-aligning, holographic phase modulation sensing device 10A of the present invention. This embodiment includes a coherent optical radiation source 16 comprised of a single mode fiber 22 emitting optical radiation that passes through collimating lens 20. Sensor 10A also includes prism 24 which acts as a beam splitter of the output from coherent optical radiation source 16 and which directs the resultant beams to phase modulation source 14 and mirror 26. In this embodiment, phase modulation source 14 is a stretched membrane of metallized plastic which vibrates when sound is present. The output of phase modulation source 14 is coupled into one of the two beams produced by prism 24, which is then redirected through Zefpr crystal 12 where it interferes with the second beam produced by prism 24 which has been directed to Zefpr crystal 12 by reflection off

mirror 26. The phase modulation of the interfering beams results in a linear variation of the transmitted intensity of the two beams through Zefpr crystal 12, which is then detected by detectors 18.

FIG. 3 shows yet another preferred embodiment of the present invention in which phase modulation source 14 is comprised of a piezo-electric mirror that introduces a phase modulation into one of the beams produced by prism 24.

FIG. 4 shows another preferred embodiment of the present invention 10B, suitable for phase image subtraction between counterpropagating input phase images. This embodiment of the present invention includes coherent optical radiation source 16, Zefpr crystal 12, first and second phase imaging transparencies 28, 30, first and second imaging lenses 32, 34, first, second and third beam splitters 36, 38, 40 and detectors 18. In this embodiment, the output from coherent optical radiation source 16 is split by first beam splitter 36 and the resultant beams are directed through first and second phase imaging transparencies 28, 30, respectively. First and second phase imaging transparencies 28, 30 modulate the beams passing through them to produce first and second input phase images, which, as represented by T_1 and T_2, are imaged on Zefpr crystal 12 by first and second imaging lenses 32, 34, and therein interact with one another. The focal depth of the lens configuration must be longer than the interaction region within the crystal.

Because of the nature of the counterpropagating geometry of the first and second input phase images, each pixel of one input image interacts with only one pixel of the other image, thereby allowing each pair of pixels to be considered independently. Because of the linear variation with phase shift of the output intensities of the beams incident on Zefpr crystal 12, when any pixel's phase is changed, the output intensity of one pixel increases at the expense of its interacting pixel. This results in a phase image subtraction between first and second input phase images T_1 and T_2 after interfering in Zefpr crystal 12. It also gives a phase

to intensity conversion that may be measured by detectors 18.

Experiments have been performed with the all-optical, self-aligning, holographic phase modulation sensor of the present invention. In particular, the embodiment of the present invention depicted in FIG. 2 has been extensively tested. The sensitivity of this device was measured as a noise equivalent pressure level of less than 15 dB sound pressure level at 6 kHz, where 0 dB is taken to be equal to 0.0002 μbar. The stretched membrane or microphone forming phase modulation source 14 in this experimental configuration responded to frequencies from 200 Hz - 20 kHz. However, the fundamental limit of the device's sensitivity is expected to be much better.

It is to be understood that the foregoing description and accompanying drawings relate only to preferred embodiments of the present invention. Other embodiments may be utilized without departing from the spirit and scope of the invention. For example, other beam splitting mechanisms, such as electro-optical beam splitters, may be utilized in place of the beam splitters identified herein. Similarly, any source or method of introducing a phase modulation into the interfering beams transmitted through Zefpr crystal 12 or the crystal's index grating may be employed. Accordingly, it is to be further understood that the description and drawings set forth hereinabove are for illustrative purposes only and do not constitute a limitation on the scope of the invention.

What is claimed is:

1. An all-optical, self-aligning, holographic phase modulation and motion sensor comprising:

a crystal exhibiting a zero electric field photorefractive effect;

a phase modulation source having a phase modulating output;

a coherent optical radiation source having an output beam;

means for splitting said output beam into first and second interference beams;

at least one optical radiation detector; and

means for coupling said phase modulating output into at least one of said interference beams and directing said first and second interference beams through said photorefractive crystal to said optical radiation detector.

2. An all-optical, self-aligning, holographic phase modulation and motion sensor as in claim 1, wherein said means for splitting said output beam is said photorefractive crystal formed into a prism.

3. An all-optical, self-aligning, holographic phase modulation and motion sensor as in claim 1, wherein said means for splitting said output beam is a prism independent of said photorefractive crystal.

4. An all-optical, self-aligning, holographic phase modulation and motion sensor as in claim 1, wherein said coherent optical radiation source is an ion laser.

5. An all-optical, self-aligning, holographic phase modulation and motion sensor as in claim 1, wherein said coherent optical radiation source is a semiconductor laser.

6. An all-optical, self-aligning, holographic phase modulation and motion

sensor as in claim 1, wherein said coherent optical radiation source is a solid state laser.

7. An all-optical, self-aligning, holographic phase modulation and motion sensor as in claim 1, wherein said coherent optical radiation source comprises the output from a single mode optical fiber collimated through a collimating lens.

8. An all-optical, self-aligning, holographic phase modulation and motion sensor as in claim 1, said means for coupling said phase modulating output into one of said interference beams further comprises a vibrating membrane attached to said photorefractive crystal.

9. An all-optical, self-aligning, holographic phase modulation and motion sensor as in claim 1, wherein said means for coupling said phase modulating output into one of said interference beams further comprises a piezo-electric mirror.

10. An all-optical, self-aligning, holographic phase modulation and motion sensor as in claim 1, wherein said means for coupling said phase modulating output into one of said interference beams further comprises a vibrating membrane having a reflective surface configured and arranged to reflect said interference beam, into which said phase modulating output is coupled, into said photorefraction crystal.

11. An all-optical, self-aligning, holographic phase modulation and motion sensor comprising:

a crystal exhibiting a zero electric field photorefractive effect;

a phase modulation source having a phase modulating output;

an argon ion laser having an output beam;

a prism for splitting said output beam into first and second interference

beams;

at least one optical radiation detector; and

means for coupling said phase modulating output into at least one of said interference beams and directing said first and second interference beams through said photorefractive crystal to said optical radiation detector.

12. A method of sensing phase modulation comprising the steps of:

forming a crystal exhibiting a zero electric field photorefractive effect;

directing a beam of coherent optical radiation through a beam splitter to form first and second interference beams;

coupling a phase modulation into at least one of said interference beams;

directing said first and second interference beams through said photorefractive crystal wherein the transmitted intensity of the two beams will vary linearly, but in opposition to each other, with the coupled phase modulation; and

detecting the resultant linearly varying beam intensities with an optical radiation detector whereby said phase modulation is converted to a proportional current modulation.

13. An all-optical, self-aligning, holographic phase modulation and motion sensor comprising:

a crystal exhibiting a zero electric field photorefractive effect;

a coherent optical radiation source having an output beam;

at least two phase imaging transparencies;

means for splitting said output beam into first and second beams and directing said first and second beams into said first and second phase imaging transparencies respectively to produce respective first and second input phase images;

at least one optical radiation detector;

means for imaging said first and second input phase images onto said zero electric field photorefractive crystal wherein phase image subtraction between said first and second input phase images occurs; and

means for directing said phase-image-subtracted first and second input phase images to said optical radiation detector.

14. An all-optical, self-aligning, holographic phase modulation and motion sensor as in Claim 13, wherein said coherent optical radiation source is an ion laser.

15. An all-optical, self-aligning, holographic phase modulation and motion sensor as in Claim 13, wherein said coherent optical radiation source is a semiconductor laser.

16. An all-optical, self-aligning, holographic phase modulation and motion sensor as in Claim 13, wherein said coherent optical radiation source is a solid state laser.

17. An all-optical, self-aligning, holographic phase modulation and motion sensor as in Claim 13, wherein said means for splitting said output beam is a prism.

18. An all-optical, self-aligning, holographic phase modulation and motion sensor as in Claim 13, wherein said means for imaging said first and second input phase images onto said crystal further comprises first and second imaging lenses.

19. An all-optical, self-aligning, holographic phase modulation and motion sensor as in Claim 13, wherein said means for directing said phase-image-subtracted first and second input phase images to said optical radiation detector further comprises first and second phase image beam splitters.

METHOD AND APPARATUS FOR ALL-OPTICAL HOLOGRAPHIC PHASE MODULATION AND MOTION SENSING

ABSTRACT OF THE DISCLOSURE

An all-optical, self-aligning, holographic phase modulation and motion sensing apparatus includes a crystal exhibiting a zero electric field photorefractive effect, a phase modulation or vibration source or mechanism, a source of coherent optical radiation, beam splitting and directing optics, and at least one optical radiation detector. The output from the optical radiation source is split into separate beams, one or all of which are phase modulated. The beams are directed through the crystal exhibiting a zero electric field photorefractive effect, and the resultant transmitted beams are detected by an optical radiation detector to provide a measurement of the phase modulation of the beams. The sensor functions in the absence of an electric field because of the unique characteristic of the crystal exhibiting the zero electric field photorefractive effect whereby if either the phase of the crystal's index grating or of the interfering beams is modulated with a phase change very much less than $\pi/2$, the intensity of the beam transmitted through the crystal varies linearly with the modulation. Such linear modulation allows crystals exhibiting the zero electric field photorefractive effect to remotely sense phase modulations or vibrations of any type in the absence of electrical signals in the vicinity of the sensor.

\patents\90204.bwk\sg